ORIGINAL ARTICLE

Modified orca predation algorithm: developments and perspectives on global optimization and hybrid energy systems

Marwa M. Emam[1] · Hoda Abd El-Sattar[2] · Essam H. Houssein[1] ⬤ · Salah Kamel[3]

Abstract

This paper provides a novel, unique, and improved optimization algorithm called the modified Orca Predation Algorithm (mOPA). The mOPA is based on the original Orca Predation Algorithm (OPA), which combines two enhancing strategies: Lévy flight and opposition-based learning. The mOPA method is proposed to enhance search efficiency and avoid the limitations of the original OPA. This mOPA method sets up to solve the global optimization issues. Additionally, its effectiveness is compared with various well-known metaheuristic methods, and the CEC'20 test suite challenges are used to illustrate how well the mOPA performs. Case analysis demonstrates that the proposed mOPA method outperforms the benchmark regarding computational speed and yields substantially higher performance than other methods. The mOPA is applied to ensure that all load demand is met with high reliability and the lowest energy cost of an isolated hybrid system. The optimal size of this hybrid system is determined through simulation and analysis in order to service a tiny distant location in Egypt while reducing costs. Photovoltaic panels, biomass gasifier, and fuel cell units compose the majority of this hybrid system's configuration. To confirm the mOPA technique's superiority, its outcomes have been compared with the original OPA and other well-known metaheuristic algorithms.

Keywords Orca predation algorithm · Global optimization · Photovoltaic · Biomass · Fuel cell · Isolated hybrid system

1 Introduction

The likelihood of rising energy distribution disparity due to renewable energy sources is significant, ensuring long-term continuous energy distribution while simultaneously reducing emits of greenhouse gases. This is why most

✉ Essam H. Houssein
essam.halim@mu.edu.eg

Marwa M. Emam
marwa.khalef@mu.edu.eg

Hoda Abd El-Sattar
eng_ha20@yahoo.com

Salah Kamel
skamel@aswu.edu.eg

1 Faculty of Computers and Information, Minia University, Minia, Egypt

2 Electrical Engineering Department, Luxor Higher Institute of Engineering and Technology, Luxor 85834, Egypt

3 Electrical Engineering Department, Faculty of Engineering, Aswan University, Aswan 81542, Egypt

researchers are working on the design and development of distributed energy resources based on the use of renewable sources (photovoltaic panels (PV), wind turbine (WT), diesel generator (DG), biomass gasifier (BG), battery bank, and fuel cell (FC), etc.), especially in rural areas, to be utilized in feeding the required loads [1]. The hybrid energy systems need to be appropriately built and sized for distributed generation microgrids to operate securely, dependably, and economically [2]. This turns determining the hybrid energy system's ideal size into an optimization issue that includes a set of objectives. In order to optimize hybrid energy systems, many techno-economic issues have been taken into account. Examples of costs taken into account in hybrid systems optimal sizing study include net present cost (NPC), energy cost (COE), annualized system cost (ASC), and life cycle cost (LCC). The main drawback of renewable energy sources is their reliance on the environment. This drawback is reduced by using hybrid energy system combinations, guaranteeing a standard power supply to the loads. This can be achieved by combining sustainable energy sources with being used if a more potent

source fails and integrating green energy sources with conventional energy sources. Several studies focus on the effectiveness of hybrid renewable energy systems and different metaheuristic optimization techniques. Most research investigations examine whether energy production can meet load demands [3]. The technical indices used as a result are the loss of power supply probability (LPSP), the loss of load expected (LOLE), loss of energy expected (LOEE), deficiency of power supply probability (DPSP), loss of load hours (LOLH), unmet load (UL), equivalent loss factor (ELF), and renewable energy fraction [3]. Currently, examining the effectiveness of hybrid renewable systems is the subject of numerous papers, as are various optimization algorithms, with the goal being to ascertain the optimal size of the system's constituent parts and enhance the critical technical and economic indicators in the system's design. Several papers have presented different operation strategies for many hybrid systems designs that apply different metaheuristics and improved optimization strategies. For example, a standalone hybrid energy system based on PV, WTs, and FC configuration has been described in [4]. This study offered a power management approach that controls the power flow between the various system parts using the metaheuristic optimization technique called the mine blast algorithm (MBA). The obtained findings of the MBA method were compared with other techniques, namely, PSO, artificial bee colony (ABC), and cuckoo search (CS). Based on the same previous system combination, the authors in [5] proposed an optimal sizing optimization strategy for a hybrid system situated in the Ataka area in the Suez Gulf region, Egypt. A novel modified algorithm based on improving the performance of the traditional Artificial Ecosystem Optimization (AEO) method called Improved Artificial Ecosystem Optimization (IAEO) is utilized for this hybrid system. The major objective functions of this hybrid system are to reduce the COE, LPSP, and excess energy while satisfying the operational constraints. To demonstrate the IAEO technique's effectiveness, a comparison of IAEO, the original AEO, PSO, Salp Swarm Algorithm (SSA), and Gray Wolf Optimizer (GWO) has been performed.

Moreover, the work in [6] developed a new hybrid system strategy based on combining the biomass system as the primary source and the FC as a backup unit. This suggested hybrid system has been offered to supply the electric power of a microgrid in a small tourist hamlet in Hurghada city, Egypt. A Multi-objective Particle Swarm Optimization (MOPSO) method minimizes the COE and the LPSP. HOMER software tool has been utilized in [7] to apply a techno-economic analysis for a new different configurations hybrid system based on PV/WT/BG/Biogas/FC/battery components. This hybrid system is developed to

be practical in rural and remote places. This work provided optimal configuration for reducing COE and NPC.

In [8], four different metaheuristic algorithms (PSO, DE, the water cycle algorithm (WCA), and GWO methods) for determining the best size for an isolated microgrid in rural locations are tested for effectiveness and adaptability. In four separate AC-coupled isolated microgrids for a distant community in South Australia, these algorithms maximize the PV, WT, DG, fuel tank, and battery energy storage capacity. In terms of capacity optimization of the system's components, the PSO and GWO algorithms produced comparable results. While the DE method was unreliable. To obtain the optimal sizing for an isolated hybrid system consisting of PV, WT, and battery units, the authors in [9] applied ten optimization methods which are simulated annealing (SA), Jaya algorithm, moth–flame optimization (MFO), GA, CS, harmony search (HS), firefly optimization algorithm (FOA), flower pollination algorithm (FPA), the simplified squirrel search algorithm (S-SSA), and the brainstorm optimization in objective space (BSO-OS) algorithm. Abd El-Sattar et al. [10] developed a hybrid algorithm, namely the Gradient Artificial Hummingbird Method (GAHA), that combines the Gradient-Based Optimizer (GBO) with the Artificial Hummingbird Algorithm (AHA). This modified GAHA method is utilized to ascertain the optimal size of PV, WT, biomass system, and battery units for a standalone area in the new Tiba city, Luxor, Egypt, considering the reducing the COE and LPSP. In [11], an enhanced Arithmetic Optimization Algorithm known as IAOA was created by updating the original AOA with the aid of the Aquila Optimizer's leading operators (AO). This developed IAOA technique was used to determine the best design scenario for a standalone hybrid system made up of PV, WT, DG, and battery units in the El Kharga region, Egypt. The authors in [12] concentrated on determining the optimal sizing for an off-grid hybrid system using a novel PV/BG/FC construction. The objective functions of the proposed method are to reduce the COE and minimize CO_2 emissions. A novel Mayfly Optimization Algorithm (MOA) has been utilized to obtain the optimal size of this hybrid system. To prove the effectiveness of the suggested MOA method, its outcomes were contrasted with those of the Sooty Tern Optimization Algorithm (STOA), Sine Cosine Algorithm (SCA), and Whale Optimization Algorithm (WOA).

Various hybrid configurations and techno-economic analysis approaches may be used to build diverse renewable systems in the best possible ways. Accordingly, researchers have discovered in recent years that metaheuristic algorithms, which are all-purpose and straightforward to use, can tackle challenging real-world problems. Because metaheuristics are very accurate and straightforward, they have drawn much attention in various

challenging optimization issues in engineering, communications, medical, and social sciences [13]. Moreover, metaheuristic algorithms are also used to improve solutions for a variety of problems, such as global optimization [14], energy applications [15], power flow systems [16], image segmentation [17, 18], deep learning-based classification [19], scheduling microgrid systems [20], economic emission dispatch (EED) problems [21], and feature selection [22, 23]. Unlike deterministic approaches, metaheuristic algorithms use randomly generated search agents and specialized operators to find the best solutions in the search space. These operators take inspiration from natural occurrences such as swarm behavior, social behavior, physical theories, and evolutionary principles. There are three primary types of metaheuristic algorithms: (a) Swarm methods contain swarm-based strategies that simulate the social behavior of groups of animals, birds, and humans; (b) evolutionary methods; and (c) natural phenomenon algorithms imitate physics and chemistry principles [24, 25]. Particle Swarm Optimization (PSO) [26], a popular algorithm in this family of algorithms, is regarded as the origin of numerous other optimization methods. For the evolution-based techniques, researchers represent various operators based on the guides of the evolution theory. The well-known evolution-based methods are the Genetic Algorithms (GA) introduced in [27] by Holland and the Differential Evolution (DE) [28]. The physics-based algorithms were driven by the principles of physics and chemistry, such as the laws of gravity and electrical charges. Several algorithms have been presented to address real-world issues based on this inspiration, for example, Gravitational Search Algorithm (GSA) [29], Multi-verse Optimizer (MVO) [30], and the Gradient-Based Optimizer (GBO) [31].

The performance of a metaheuristic algorithm typically refers to the level of the optimized solution, and the time needed for the algorithm to converge. Even though many MAs have produced good results, optimization issues have grown more complex (as the number of optimized variables has grown) while still adhering to various constraints and requirements. However, despite the advantages of algorithms, numerous existing metaheuristic algorithms only sometimes guarantee the globally optimum solution. In addition, in solving the problems of conducting the parameters of the hybrid energy systems, no algorithm can be considered the better quality in determining the optimal sizing of an isolated hybrid system with reducing the COE within the limitations of LPSP. Therefore, developing new metaheuristic algorithms can effectively handle the issue of computing the optimal sizing for an off-grid hybrid system comprising PV/BG/Hydrogen Tank units (HT)/FC/Electrolyzer (ELE) modules. The hybridization concept of two or more metaheuristics and modified or improved existing

algorithms effectively addresses the current optimization challenges [32]. Although hybridization enhances the performance of optimization, it must be carried out with suitable algorithms. So choosing the algorithms is a crucial step. Moreover, it is standard to choose them based on how well they function independently.

Therefore, to develop a more effective algorithm used for solving the hybrid energy system problems, we have studied more recent algorithms and features. In particular, Orca Predation Algorithm (OPA) is a novel algorithm that has begun to attract interest. The OPA algorithm has several advantages. The performance of OPA is evaluated using 23 well-known unconstrained benchmark functions, recent CEC2015 and 2017 benchmark functions, and five constrained engineering issues. Although the OPA algorithm has achieved encouraging results, it is not entirely impervious to the flaws that metaheuristics may experience. Indeed, despite being effective and powerful optimization tools, metaheuristics can run into problems. Nonetheless, any original metaheuristic algorithm has some drawbacks that impair functionality and cause slow convergence or trapping in local optima. As a result, these algorithms must be enhanced by changing the original method [33] or combining two algorithms to adjust the search techniques [34, 35]. According to the optimization problem, the main problems mentioned in the studies are the algorithm's slow convergence speed, its tendency to get stuck in local optima, how much algorithm parameters affect algorithm performance, and how poorly exploration and exploitation are balanced. So, this paper proposes a modified Orca Predation Algorithm (mOPA) to address these limitations. The Lévy flights (LF) strategy has shown good results in enhancing metaheuristics performance [36]. Also, OBL [37] is one of the most beneficial methods for improving the search performance of the metaheuristics [38]. The mOPA method was utilized to compute the optimal sizing for an off-grid hybrid system comprising PV/BG/Hydrogen Tank units (HT)/FC/Electrolyzer (ELE) modules to demonstrate this modified approach's usefulness. The results obtained from utilizing the mOPA are compared with results from the original OPA method and other techniques used in [12] for the same hybrid system. This work brought attention to the possibilities of using biomass systems with fuel cell technology for energy storage. Utilizing recent developments in data science and modeling methodologies, which give the required technical tools for informing decision-making, will help to enable the successful realization and deployment of these sophisticated technologies.

The contributions of the paper are summarized in the following points:

– This paper proposed an improved mOPA algorithm that combines two enhancing strategies: Levy flight and OBL.
– mOPA is applied to solve global optimization problems. Moreover, we compare its performance with different well-known metaheuristic algorithms.
– The performance of mOPA compared to competitors is demonstrated using the CEC'20 test suite problems.
– The proposed mOPA is applied to develop an optimal design for an isolated hybrid PV/BG/HT/FC/ELE system for supplying a load in Abu-Monqar region, located in Egypt.
– The proposed mOPA method is used to solve the problem of reducing the COE, within the limitations of LPSP.
– To prove the superiority of the recommended mOPA technique for the suggested optimization problem, the mOPA results compared with other well-known algorithms (Mayfly optimizer (MOA), Sooty Tern optimizer (STOA), and Sine Cosine optimizer (SCA)).

This paper is structured as follows: Section 2 describes the mathematical model for the original OPA method required to construct the suggested modified algorithm, the OBL concept, and the Lévy flight method. The mathematical model of the suggested mOPA algorithm is presented in Sect. 3. Section 4 discusses the real-world application, divided into four subsections. These subsections describe the suggested hybrid system components design, the optimization problem formulation, the operation energy management strategy, and the description of the site of the project study, respectively. Section 5 discusses the design findings, and the discussion contains the performance results of the proposed mOPA on CEC'20 benchmark functions and the results of the proposed hybrid system. Finally, Section 6 provides this paper's conclusion and future work.

2 Preliminaries

This section will discuss the techniques essential to building the proposed method. The original Orca Predation Algorithm (OPA) mathematical model and the OBL idea, and the Lévy flight technique are described in detail.

2.1 Orca predation algorithm (OPA)

OPA is a novel bio-inspired metaheuristic algorithm developed by Yuxin et al. [39]. It mimics the hunting manners of orcas and simplifies it into three phases: driving, encircling, and attacking phase. OPA gives various qualities to the driving and encircling in parameter

modification to balance the exploitation and exploration processes. In the attacking phase, the best solution may be determined without sacrificing the particles' variety after considering the positions of many best orcas and several randomly chosen orcas.

The detailed mathematical formulations of the OPA algorithm are as follows:

1. *Development of a colony of orcas* A group of N_n oracs are used in OPA and represent in $1D$, $2D$, $3D$, or extra-dimensional space. It is represented in Eq. 1

$$X = [x1, x2, x3, ..., xN_n] = \begin{bmatrix} X_{1,1} & X_{1,2} & \ldots & X_{1,\text{Dim}} \\ X_{2,1} & X_{2,2} & \ldots & X_{2,\text{Dim}} \\ \vdots & \vdots & \vdots & \vdots \\ X_{N_n,1} & X_{N_n,2} & \ldots & X_{N_n,\text{Dim}} \end{bmatrix}$$
(1)

where X denotes the orca population of the candidate solutions. xN_n denotes the position of the Nth individual orca, and xN_n, Dim is the position of the Dim^{th} dimension of the Nth population.

2. *Chasing phase* This phase is divided into two steps: driving and encircling. p_1 is used to adapt the probability of the orca performing these two steps individually. It is a constant in [0, 1], and a random number is generated between [0, 1]. If this random number is greater than p_1, the driving process is applied; other else, the encircling process will be applied.

3. *Driving process* In order to prevent the orca group from straying from the target, it is also vital to regulate the orca group's central position and keep it near to the prey. The moving speed of the orca and the relevant position is shown in the following equations:

$$V_{\text{chase},1,i}^t = a \times (d \times x_{\text{best}}^t - F \times (b \times M^t + c \times x_i^t))$$
(2)

$$V_{\text{chase},2,i}^t = e \times x_{\text{best}}^t - x_i^t$$
(3)

where t indicates the number of iterations, $V_{\text{chase},1,i}^t$ represents the chasing speed after choosing the first chasing step. $V_{\text{chase},2,i}^t$ represents the chasing speed after choosing the second chasing. Moreover, a, b, and d are randoms in [0, 1]. e is a random value in [0, 2], F is equal to 2, and q is in [0, 1] that used for choosing the chasing technique. While, M indicates the average location of the orca population as shown in Eq. 4.

$$M = \frac{\sum_{i=1}^{N_n} x_i^t}{N_n}$$
(4)

$$c = 1 - b \tag{5}$$

There are two chasing methods depending on the orca population size. If the orca is large, i.e. $(rand > q)$, the first process is applied; otherwise, if $(rand \leq q)$, the second process is applied as shown in Eq. 6.

$$\begin{cases} x_{\text{chase},1,i}^{t} = x_i^t + V_{\text{chase},1,i}^{t} & if \quad rand > q \\ x_{\text{chase},2,i}^{t} = x_i^t + V_{\text{chase},2,i}^{t} & if \quad rand \leq q \end{cases} \tag{6}$$

4. *Encircling of prey* In this step, the orcas updating using the positions of three randomly orcas that can be expressed as follows:

$$x_{\text{chase},3,i,k}^{t} = x_{d1,k}^{t} + u \times \left(x_{d2,k}^{t} - x_{d3,k}^{t} \right) \tag{7}$$

$$u = 2 \times (randn - 1/2) \times \frac{\text{Maxitr} - t}{\text{Maxitr}} \tag{8}$$

where *Maxitr* is the maximum iteration numbers, $d1$, $d2$, and $d3$ represent the three randomly selected orcas from N_n orcas and $d1 \neq d2 \neq d3$. $x_{\text{chase},3,i}^{t}$ is the position after selecting the third chasing technique.

5. *Position changes during the encircling phase* The positions are adjusted according to the following equations:

$$\begin{cases} x_{\text{chase},i}^{t} = x_{\text{chase},i}^{t} & IF \quad f\left(x_{\text{chase},i}^{t}\right) < f\left(x_i^t\right) \\ x_{\text{chase},i}^{t} = x_i^t & IF \quad f\left(x_{\text{chase},i}^{t}\right) \geq f\left(x_i^t\right) \end{cases} \tag{9}$$

where $f(x_{\text{chase},i}^{t})$ is the fitness function relevant to $x_{\text{chase},i}^{t}$, and $f(x_i^t)$ is the fitness function relevant to x_i^t.

6. *Attacking of prey* The four best-attacking positions in a circle are represented by four orcas. The following equations are used to determine the orca's movement speed and location during an attack.

$$V_{\text{attack},1,i}^{t} = \left(x_1^t + x_2^t + x_3^t + x_4^t \right)/4 - x_{\text{chase},i}^{t} \tag{10}$$

$$V_{\text{attack},2,i}^{t} = \left(x_{\text{chase},d1}^{t} + x_{\text{chase},d2}^{t} + x_{\text{chase},d3}^{t} \right)/3 - x_i^t \tag{11}$$

$$x_{\text{attack},i}^{t} = x_{\text{chase},i}^{t} + g_1 \times V_{\text{attack},1,i}^{t} + g_2 \times V_{\text{attack},2,i}^{t} \tag{12}$$

where $V_{\text{attack},1,i}^{t}$ and $V_{\text{attack},2,i}^{t}$ are the speed vectors, $x_1^t, x_2^t, x_3^t, and\ x_4^t$ are the four orcas in the best position, $d1, d2, and\ d3$ are the three randomly choosen orcas from N_n in the chasing step and $d1 \neq d2 \neq d3$, $x_{\text{attack},i}^{t}$ identifies the position after the attacking process, g_1 is a random number in [0, 2], and g_2 is a random number in $[-2.5, 2.5]$.

7. *Position changes during the attacking phase* The position of the orca is determined by the lower boundary l_b of the problem that can be identified using the following scheme:

If $f(x_{\text{attack},i}^{t}) < f(x_{\text{chase},i}^{t})$

$\quad X_i^{t+1} = x_{\text{attack},i}^{t}$

Else

$\quad Q = randn$

$\quad$ For K from 1 to D

$\quad\quad$ If $Q < p2$

$\quad\quad\quad x_{j,k}^{t+1} = l_b(k)$

$\quad\quad$ Else

$\quad\quad\quad x_{j,k}^{t+1} = x_{\text{chase},i,k}^{t}$

$\quad\quad$ End

$\quad$ End

End

$$\tag{13}$$

where $p2$ is a value in [0, 1].

To conclude, the following steps illustrate the implementation of the OPA algorithm

- **Step 1:** Initialize the parameters and orca populations; number of population N_n, dimension *Dim*, maximum number of iterations *Maxitr*, selection probability $p1$, $p2$, lower bound l_b, and upper bound u_b. The positions of orcas are defined randomly using l_b and u_b.
- **Step 2:** Each orca's fitness value is determined, and the optimal fitness is selected as X_{best}.
- **Step 3:** The orca group's position is being updated during the chasing phase. Depending on the selection factor $p1$, orcas decide whether to drive or encircle the prey at this stage. The positions are updated as shown from Eqs. 2 to 9.
- **Step 4:** The orcas changed their positions throughout the attacking phase. The positions are updated using Eqs. 10–12, and their positions are then replaced by l_b as shown in Eq. 13.
- **Step 5:** After the attacking process, the new population will be expanded into a new group.
- **Step 6:** Termination criteria: the process is terminated if the current iteration number exceeds the allowed number of iterations. Step 2 of the preceding procedures will be repeated if the optimal output solution is not reached.

2.2 Opposition-based learning (OBL)

Metaheuristic algorithms often begin with a random initial population, and over-optimization process iterations,

population agents increase the chance of reaching the best solutions. Since these algorithms have a stochastic nature, the convergence time is mainly related to the distances between the initial guesses and the promising or optimal solution. As a result, the more used initial solutions close to the best solution, the more the metaheuristic algorithm quickly converges through problem search space and vice versa. OBL is a metaheuristic optimization technique used to improve a search algorithm's convergence rate. It is an effective technique to prevent stagnation in candidate solutions [37]. The main idea of OBL is to evaluate candidate solutions in pairs, with one solution representing the current best solution and the other solution representing the "opposition" or "antithesis" to the current best solution. Comparing these two solutions allows the algorithm to identify promising areas of the search space more quickly, thereby speeding up the convergence process toward an optimal solution. HR. Tizhoosh developed the idea of the OBL [40]. OBL improves the exploitation ability of a search mechanism. In metaheuristics, convergence typically occurs when the initial solutions are nearer the optimal site; otherwise, late convergence is anticipated. By considering opposing search regions, which may be nearer to the global optimum, the OBL technique discovers better solutions in this case. The OBL works by traversing the search space in both directions. These two approaches make use of one of the initial solutions, while the opposite approach establishes the other path and then takes the most optimal solution [41]. The following describes the concept of OBL:

- *Opposition number* OBL is defined as being explained by the concept of opposite numbers. The following expressions can present the opposition-based number. Consider $\dot{x}$ is a real number belongs to the range $[u, w]$, $[u, w] \in R$, the opposite number of $\dot{x}$ is defined by Eq. (14) [41]

$$\bar{x} = u + w - \dot{x} \tag{14}$$

- *Opposition point* Assuming, $P_x = \dot{x_1}, \dot{x_2}, \dot{x_3}, ..., \dot{x_D}$ be a point in D-dimensional space, where $\dot{x_i} \in [u_i, w_i]$, $u_i, w_i \in R$, $i = 1, 2, 3,..., D$. The point $(\overline{P_x})= \overline{x}_1, \overline{x}_i, ..., \overline{x}_D$. All items in $\overline{x}$ computed by Eq. (15)

$$\overline{x}_j = u_j + w_j - \dot{x}_j \quad where \quad j = 1, 2, 3, ..., D \tag{15}$$

- *The Opposition in optimization* In the optimization method, the opposite number $\bar{x}$ is replaced by the equivalent point $\dot{x}$ according to the objective function. If $f(\dot{x})$ is better than $f(\bar{x})$, then $\dot{x}$ not replaced; otherwise, $\dot{x}$

$= \bar{x}$, so, the solutions of the population are updated according to the best value of $\dot{x}$ and $\bar{x}$ [42].

In OBL, the optimization process is completed using the solution with the best fitness determined by simultaneously evaluating both current candidate and opposition-based solutions. This comparison process helps to increase the speed at which the optimizer converges to promising solutions.

2.3 Lévy flight (LF)

Paul Lévy proposed the LF, and Benoit Mandelbrot elaborated on it. The step lengths in LF follow a probability distribution with hefty tails. It is one of the most common flight patterns in naturally occurring surroundings [43]. The step sizes of LF calculated using the probability function as shown in Eq. (16) [44]:

$$L(x_j) \approx |x_j|^{1-\alpha} \tag{16}$$

where x_j denotes the flight length, and $(1 < \alpha \leq 2)$ is the power exponent. The probability density of Lévy step in integral form is shown in Eq. (17):

$$f_v(x; \alpha, \rho) = \frac{1}{\pi} \int_0^\infty \exp(-\rho q^\alpha) \cos(qx) dq \tag{17}$$

α decides the distribution index, and ρ sets the scale unit. When $(\alpha = 2)$, it signifies Gaussian distribution, and when $(\alpha = 1)$, it signifies a Cauchy distribution [45]. Equation (17) uses a series expansion technique only when x has a vast value as Eq. (18):

$$f_v(x; \alpha, \rho) \approx \frac{\rho \, \Gamma(1 + \alpha) \, \sin\left(\frac{\pi\alpha}{2}\right)}{\pi \, x^{(1+\alpha)}}, \quad x \to \infty \tag{18}$$

where Γ is the gamma function.

For an index distribution, α value between 0.3 and 1.99 is a practical approach to generate a Lévy stable process. Mantegna *et al.* [46] creates random numbers method based on the Lévy distribution by Eq. 19:

$$levy(\alpha) = 0.05 \times \frac{x}{|y|^{1/\alpha}} \tag{19}$$

where x and y represent normal distribution parameters with the standard deviations of σ_x and σ_y given in Eqs. (20 and 22).

$$x = \text{Normal}(0, \sigma_x^2) \tag{20}$$

$$y = \text{Normal}(0, \sigma_y^2) \tag{21}$$

$$\sigma_x = \left[\frac{\Gamma(1+\alpha)\sin\left(\frac{\pi\alpha}{2}\right)}{\Gamma\left(\frac{(1+\alpha)}{2}\right)\alpha\, 2^{\frac{(\alpha-1)}{2}}} \right]^{1/\alpha} , \sigma_y = 1, \alpha = 1.5 \qquad (22)$$

3 The proposed mOPA algorithm

This section provides the proposed mOPA algorithm in detail. mOPA is proposed to enhance search efficiency and avoid the limitations of the original OPA.

3.1 Shortcomings of mOPA

The original OPA algorithm has shown good performance in solving global and real-world optimization problems. However, it suffers from the lack of exploration problem as it searches inside the search region identified by the orcas. This behavior of the basic OPA algorithm stuck the whole population into local optima and may lead the algorithm to premature convergence, especially in complex and high-dimensional problems. So, referring to the No Free Lunch (NFL) that promotes the concept that no stronger optimization algorithm can perform well at all the optimization problems. Therefore, the Lévy flight strategy and the OBL mechanism have been introduced in the proposed mOPA algorithm to overcome the shortcomings of the original OPA.

3.2 Initialization phase of mOPA

According to the OPA algorithm, the mOPA algorithm begins by developing an initial population (N_n); each population has a dimension (Dim) in the search space limited by the lower and upper boundaries (l_b and u_b). The positions of orcas are defined according to l_b and u_b as shown in Eq. 23 in addition to the maximum number of iterations *Maxitr* and the selection probability $p1$ and $p2$.

$$Xb_i = lb_i + rand \times (ub_i - lb_i); \ i = 1, 2, ..., N_n \qquad (23)$$

Then, the mOPA's diversity was improved in the search process using the OBL strategy during the initialization phase to enhance the search operation by Eq. 24:

$$\text{Opp}_s = l_b + u_b - x_b, b \in 1, 2, ..., N_n \qquad (24)$$

where Opp_s is a vector obtained by performing the OBL.

3.3 The fitness evaluation phase of mOPA

Each orca's fitness value is determined, and the best one is selected as X_{best}.

3.4 Chasing phase

This phase is divided into two steps: driving and encircling process. p_1 is used to adjust the probability of the orca performing these two steps individually. It is a constant in [0, 1], and a random number is generated between [0, 1]. If this random number is greater than p_1, the driving phase is applied; other else, the encircling phase will be applied.

3.4.1 Perform the LF

LF is applied to acquire new positions during the chasing phase in the driving step using the following equations:

$$\text{VL}^t_{\text{chase,1,i}} = a \times \left(d \times x^t_{\text{best}} - F \times \left(b \times levy(\alpha)^t + c \times x^t_i \right) \right) \qquad (25)$$

$$\text{VL}^t_{\text{chase,2,i}} = levy(\alpha) \times x^t_{\text{best}} - x^t_i \qquad (26)$$

There are two chasing methods based on the orca population size as illustrated in Eq. 27.

$$\begin{cases} x^t_{\text{chase,1,i}} = x^t_i + \text{VL}^t_{\text{chase,1,i}} & if \quad rand > q \\ x^t_{\text{chase,2,i}} = x^t_i + \text{VL}^t_{\text{chase,2,i}} & if \quad rand \le q \end{cases} \qquad (27)$$

3.4.2 Encircling step

After applying the LF strategy in the previous step, the position updated using equations from Eqs. 7 to 9 as shown in Sect. 2.1.

3.5 Attacking phase

The orcas changed their positions throughout the attacking phase as disscussed in Sect. 2.1. The positions are updated using Eqs. 10–12, and their positions are then replaced by lower bounds l_b as shown in Eq. 13.

3.6 Termination criteria of mOPA

The proposed mOPA optimization process is repeated until the stopping criteria is met. The pseudo-code of the proposed mOPA algorithm is provided in Algorithm 1. Also, the flowchart of the mOPA algorithm is presented in Fig. 1.

Algorithm 1 Pseudo-code of the proposed mOPA algorithm.

Input: population size N_n, maximum iterations $Maxitr$, l_b, u_b, Dimension Dim.

Output: The best solution.

Initialize OPA parameters: $p1 = 0.1$, $F = 2$, $q = 0.9$.

Randomly initialize the orca population X with dimensions dim using Eq. 1.

while (t < $Maxitr$) **do**

    for $ith\ orca\ from\ 1\ to\ N_n$ **do**

        $X_i = l_b i + rand \times (u_b i - l_b i)$

        Perform OBL on the initial population by Eq. (24) and save result in Opp_s.

        Evaluate X_i using the fitness function and store results in fit_i.

        Compute the fitness value.

        if $Fit_i < FitOpp_i$ **then**

            $X_i = Opp_i$;

        end if

    end for

    Calculate the Fitness Function for the candidate solutions (X).

    Find the Best solution so far.

    for $i = 1\ to\ N$ **do**

        if rand > p1 **then**

            if rand > q **then**

                Perform Levy flight; Obtain the new positions X_{chase} by equations Eq. 25 and Eq. 27

            Else

                Perform Levy flight; Obtain the new positions X_{chase} by equations Eq. 26 and Eq. 27

            end if

            Update the positions according to evaluate the fitness functions using Eq. 9

        Else

            Obtain the new positions X_{attack} by equations Eq. 10, Eq. 11, and Eq. 12

        end if

        Update positions using Eq. 13

    end for

    $t = t + 1$

end while

Return the best solution.

---

4 Real-world application

4.1 The proposed hybrid system design

In order to service a tiny remote area in Egypt, an off-grid hybrid system is simulated and evaluated to determine the best size and satisfy the electricity demand while reducing costs. This hybrid system's primary components are PV, BG systems, ELE units, HT, and FC, which is described in detail as below:

4.1.1 Photovoltaic solar module (PV)

The following equations can be utilized to compute the PV array's generated power $P_{PV}(t)$ and cell temperature T_{CELL} [47–49]:

$$P_{PV}(t) = \left(\frac{ISR(t)}{1000}\right)\left(N_{PV}P_{PV}^{rat}\eta_w\eta_{PV}\right)\left(1 - T_\gamma(T_{CELL} - 25)\right) \tag{28}$$

$$T_{CELL}(t) = ISR(t)((T_N - 20)/800) + T_A \tag{29}$$

$ISR(t)$ is the solar radiation intensity that is present at any given time (t), N_{PV} is the PV units number, P_{PV}^{rat} is the PV rated power, η_w is the wiring efficiency, and η_{PV} is the PV module efficiency. While T_γ, T_N, and T_A are the maximum power temperature coefficient for PV modules, the cell temperature at normal operating conditions, and the ambient temperature, respectively. The main characteristics of the PV and inverter unit are indicated in Table 1.

4.1.2 Biomass system (BG)

A small-scale downdraft gasification technique was employed in this study, which transforms solid biomass into a gaseous fuel (called producer gas or syngas) that is used to power turbines. The system performance can be expressed as follows [50–52]:

$$\eta_{Sy} = (LHV_{Sy}m_{Sy})/(LHV_B m_B) \tag{30}$$

$$P_G(t) = (N_{BG}/F_m)\left(\frac{\eta_{sy}LHV_B B_{rat}(t)}{LHV_{sy}} - F_0 P_{G_{rat}}\right) \tag{31}$$

$$F_{BG}(t) = (LHV_{sy}/(\eta_{sy}LHV_B))(N_G F_0 P_{G_{rat}} + F_m P_G(t)) \tag{32}$$

$$E_{BG} = P_G(GF * 8760) \tag{33}$$

The following expression is used to describe the amount of power produced from renewable sources P_{RS}:

$$P_{PV}(t) + \left(\frac{P_G(t)}{\eta_{inv}}\right) \tag{34}$$

where η_{Sy} is the producer gas efficiency. LHV_{Sy} and LHV_B are, respectively, the product gas's and biomass material's lower heat values. m_{Sy} and m_B are the mass of the producer gas flowing and the biomass material, respectively. N_{BG} is the biomass generators number, P_G is hourly biomass consumption rate, $B_{rat}(t)$ is the rated power of biomass generators, P_{Grat} denotes the rated power of biomass generators, and F_m and F_0 represent, respectively, the marginal and no-load fuel usage. $F_{BG}(t)$ is the generator rated power, E_{BG} presents the yearly (8760 hours) power generated by the biomass generator, and GF denotes the gasifier utilization factor. The main characteristics of the BG unit are indicated in Table 2.
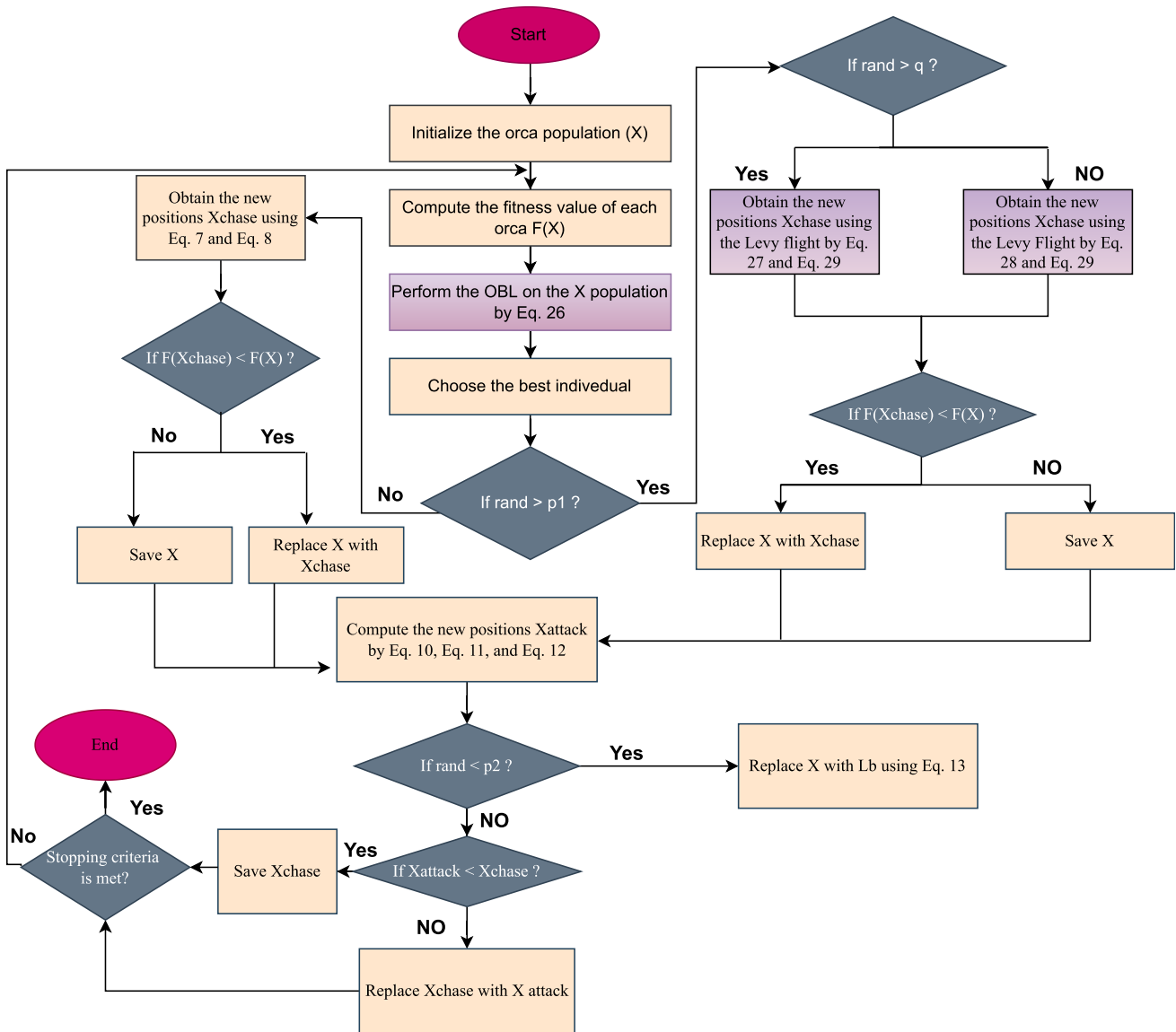
Fig. 1 Flowchart of mOPA algorithm

4.1.3 Electrolyzer (ELE), hydrogen tank unit (HT), and fuel cell (FC) modeling

The electrolyzer (ELE) is a technology that uses an electric current to pass through the liquid, creating a chemical reaction. In this study, a water ELE is used in order to produce ultra-pure hydrogen in an unpolluted manner, where the hydrogen gas is produced and collected at a pressure of 30 bar [53]. This hydrogen cannot be transferred directly to the FC because the reactant pressures within it are up to 1.2 bar [53]. Therefore, a hydrogen tank is used to link directly with the ELE [7, 54]. Following the process of separating hydrogen and oxygen, the hydrogen gas is moved and saved in HT before being utilized in the

FC to produce energy. The energy transferred to the HT from the ELE ($P_{ELE/HT}$) is stated as [5, 53]:

$$P_{ELE/HT} = \eta_{ELE} * P_{RS/ELE} \qquad (35)$$

where η_{ELE} indicates the ELE efficiency, and $P_{RS/ELE}$ symbolizes the renewable energy that powers the ELE. The lowest and highest parameters constrain the stored hydrogen mass in the HT (m_{HT}) during the operation [5], according to this formulation:

$$m_{HT}^{min} \leq m_{HT}(t) \leq m_{HT}^{max}, \qquad (36)$$

The hydrogen power ($P_{HT}(t)$) and $mHT(t)$ kept in the HT at a time interval (t) are stated as follows [7, 55]:

Table 1 Main characteristics of the PV and inverter units

Parameter	Value	Unit
PV system		
PV panel cost	14,854	$/m$\hat{2}$
T_γ	0.0037	–
η_{PV}	15	%
Rated power	1	kW
Length	1625	Mm
Width	1019	Mm
Thickness	46	Mm
PV modules lifespan	20	year
PV replacement cost	13,885	$
Inverter unit		
Efficiency	95	%
Inverter lifespan	15	year
Inverter capital cost	800	$/unit
Replacement cost	750	$/kW
Operating and maintenance cost	8	$/unit-year

$$P_{HT}(t) = P_{HT}(t-1)\left(P_{ELE/HT}(t) - \left(\frac{P_{HT/FC}(t)}{\eta_{HT}}\right)\right) * \delta t \quad (37)$$

$$m_{HT}(t) = P_{HT}(t)/HHV_H \quad (38)$$

where $P_{HT/FC}(t)$ is the power that the HT sends to the FC, η_{HT} is the efficiency of the HT, δt is the simulation's time period, and HHV_H is the stored hydrogen gas's higher heat value. The major characteristics of the ELE, HT, and FC units are indicated in Table 3. Depending on the fuel cell's total efficiency (η_{FC}), the amount of electricity that FC produces (P_{FC}) can be stated as follows [7, 55]:

Table 2 Major characteristics of the biomass system

Factor	Value	Unit
LHV_B	14.8	MJ/kg
LHV_{sy}	4.766	MJ/kg
P_{rat}	72	kg/h
η_{sy}	80	%
P_{Grat}	40	KW
F_0	0.0644	kg/h/50 kW
F_m	0.2998	kg/h/50 kW
Capital cost	23,700	$/kW
Replacement cost	15,000	$/unit
lifespan	25,000	h
Operating and maintenance cost	0.05	$/h

$$P_{FC} = \eta_{FC} * P_{HT/FC} \quad (39)$$

4.2 The optimization issue formulation

4.2.1 Objective function

The main objective purpose of this system is to minimize the COE and estimate the chance of insufficient power supply operation using the LPSP, and minimizing the dummy load's (L_{dum}) consumption of extra energy (P_{EX}) to keep the system's cost as low as possible. The values of the objective functions are determined using the following expressions [5, 56]:

$$Min_Z(F) = Min(\alpha_1 COE + \alpha_2 LPSP + \alpha_3 P_{EX}) \quad (40)$$

$$Z = [N_{PV} N_{BG} m_{HT} P_{ELE/HT} P_{FC}] \quad (41)$$

$$LPSP = \sum_1^{8760}\left(\frac{P_{dem}(t) - P_{RS}(t) - P_{FC}(t)}{P_{dum}(t)}\right) \quad (42)$$

$$P_{EX} = \sum_1^{8760}\left(\frac{L_{dum}}{P_{dem}}\right) \quad (43)$$

α indicates the value of each objective function's weight factor ($\alpha_1 = 0.3$, $\alpha_2 = 0.5$, and $\alpha_3 = 0.2$), Z stands for the optimization problem's control variables, and $p_{dem}(t)$ is the power load demand (kWh).

4.2.2 Constraints

According to the decision variables' higher and lower bounds, the optimization method operates within the limitations listed below:

$$1 \leq N_{PV} \leq N_{PV}^{max}, \quad (44)$$

$$1 \leq N_{BG} \leq N_{BG}^{max}, \quad (45)$$

$$1 \leq m_{HT} \leq m_{HT}^{max}, \quad (46)$$

$$1 \leq P_{ELE/HT} \leq P_{ELE/HT}^{max}, \quad (47)$$

$$1 \leq P_{FC} \leq P_{FC}^{max}, \quad (48)$$

$$LSPS \leq 0.06, \quad (49)$$

N_{PV}^{max} and N_{BG}^{max} represent the max items of PV modules and the generators, respectively. m_{HT}^{max} is the HT's maximum capacity (kg). $P_{ELE/HT}^{max}$ and P_{FC}^{max} represent the ELE's and the FC's units' maximum ratings (kW), respectively.

Table 3 Main characteristics of the ELE, HT, and FC

Parameter	Electrolyzer unit	Hydrogen tankuUnit	Fuel cell unit	Unit
Rated power	1	1	1	kW
Lifetime	20	20	5	year
Efficiency	75	95	50	%
Capital cost	2000	1300	3000	$/unit
Replacement cost	1500	1200	2500	$/unit
Operating and maintenance cost	25	15	175	$/unit

4.2.3 Cost analysis

The total COE, which is created by microgrid components, is regarded as an objective function that should be reduced in this work. The hybrid microgrid's total annual cost (TAC), the NPC ($), and COE ($/kWh) are expressed as follows:

$$\text{COE} = \left(\frac{\text{NPC}}{\sum_1^{8760} P_{\text{dem}}} \right) * \text{CRF} \tag{50}$$

$$\text{NPC} = \left(\frac{\text{TAC}}{\text{CRF}} \right) \tag{51}$$

$$\text{CRF}(r, s) = \left(\frac{r(r+1)^s}{(r+1)^s - 1} \right) \tag{52}$$

$$\text{TAC} = \sum_1^{8760} C_{\text{OM}}^y + \sum_1^{8760} C_{\text{rep}}^y + C_{\text{an-cap}}^y + C_{\text{an-fuel}} \tag{53}$$

where CRF indicates the capital recovery parameter, r represents the interest rate ($r = 6$ %), and s denotes the lifespan of the proposed hybrid system ($s = 25$ years). C_{OM}^y represents the total operation and maintenance cost for each component (PV, BG, ELE, HT, and FC), C_{rep}^y is the total replacement cost for each unit, $C_{\text{an-cap}}^y$ denotes the annualized cost of each subsystem, and $C_{\text{an-fuel}}$ is the biomass unit's annual fuel costs.

4.3 Operation energy management strategy

The three key cases that make up the operational strategy of the suggested hybrid system are as follows and are indicated in Fig. 2 which shows its flowchart:

1. When the power generation produced from renewable sources (PV and BG) $P_{\text{RS}}(t)$ covered the load requirement, in this situation, the produced power is delivered to satisfy the necessary load demand p_{dem}, and no power is required from the FC or supplied to the ELE;
2. The ELE will be fed with excess energy when the amount of renewable energy produced exceeds the load

requirement; the hydrogen produced from this process is then utilized to charge the HT units;
3. In this situation, the FC will utilize hydrogen contained in the HT to compensate for the lack of energy production when the power generated from renewable sources is not enough to fulfill the load requirement. Once the HT capacity is at its lowest point, there is a loss of load.

4.4 The site of the project study

The suggested hybrid system is located in Abu-Monqar region, Egypt, as indicated in the map in Fig. 3. Figures 4, 5, 6, and 7 indicate the profile load and the meteorological conditions.

5 Design results and discussion

Before applying the proposed mOPA to estimate the optimal sizing for an off-grid hybrid system comprising PV/BG/HT/FC/ELE modules, we assess its efficiency at the IEEE Congress on Evolutionary Computation 2020 (CEC 2020) [57]. The proposed mOPA's results are compared with those obtained with WOA [58], SCA [59], the Tunicate Swarm Algorithm (TSA) [60], the Slime Mold Algorithm (SMA) [61], the Harris Hawk Optimization algorithm (HHO) [62], the Runge Kutta optimization algorithm (RUN) [63], and the original OPA. We choose
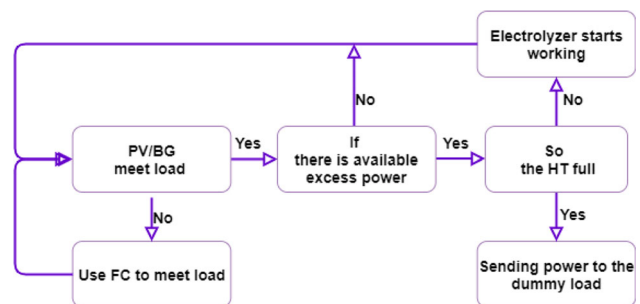

Fig. 2 The suggested hybrid system's strategy diagram

Fig. 3 Map location of Abu-Monqar region, Egypt
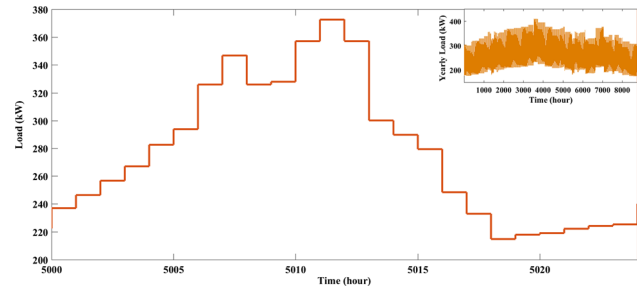

Fig. 4 The profile of the daily and annual load
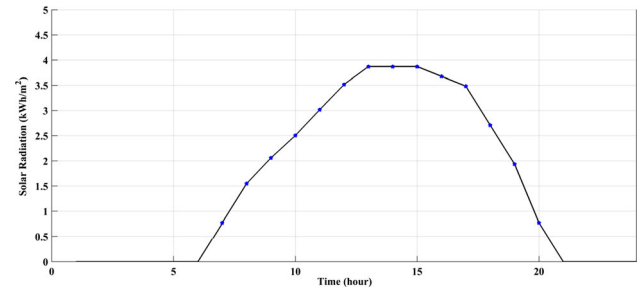

Fig. 5 Average daily PV radiation measured per hours
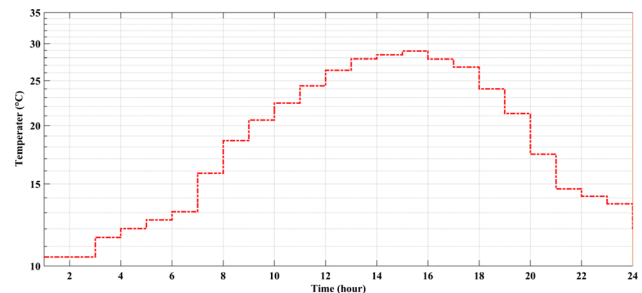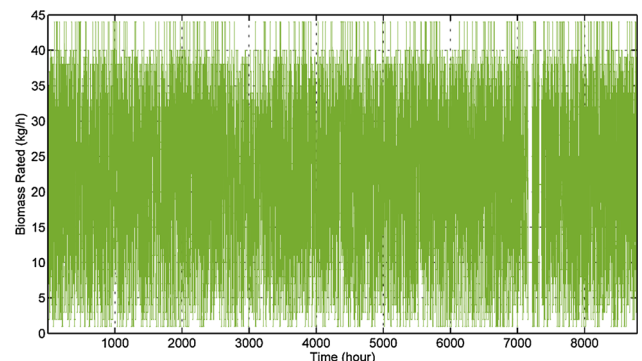

Fig. 6 Average daily PV temperature per hours

Fig. 7 The quantity of biomass consumed annually

the comparing algorithms according to different criteria, such as the size and complexity of the optimization problem and the algorithms' convergence speed. In addition to the robustness of the optimization algorithms, these comparison algorithms have recently gained much popularity in several engineering and complex applications fields and have already been applied to the same problem.

5.1 Parameter settings

The algorithm settings are shown in Table 4. Since the study in [64] demonstrates that default values are an appropriate parametrization for algorithm comparison, we set them to their default values. Additionally, default values reduce the possibility of comparison bias because no algorithm might benefit from improved tuning. Simulation is independently run 30 times to ensure fair benchmarking comparison. Both qualitative and quantitative measurements assess the efficiency of algorithms. Experiments are done using "Windows 10 (64 bit)" running on "CPU Core i7 with 8 GB of RAM," and "Matlab 2016b" is used.

5.2 Performance of the proposed mOPA on CEC'20 benchmark functions

5.2.1 CEC'20 benchmark functions

We used the benchmark functions of the CEC'20 [57] to validate the performance of the proposed algorithm since they are among the most recent benchmarks and are challenging to solve. Table 5 presents the CEC'20 functions with their corresponding optimum valußes "Fi*" [65].

Figure 8 illustrates in two dimensions the different shapes of the CEC'20 functions.

5.2.2 Statistical results analysis

This subsection presents the comprehensive results and comparisons demonstrating the basic exploratory and exploitation of mOPA compared with OPA and other well-known algorithms. Table 6 reports the mean fitness, standard deviation, and best and worst results for mOPA compared with other algorithms over 10 CEC'20 test functions with a dimension (Dim = 10). The best values (minimum) are highlighted in bold. As demonstrated in Table 6, the proposed mOPA algorithm achieves the optimal value for the unimodal F-1 test function. While for multi-modal functions F-2, F-3, and F-4, RUN gives the optimal value on the F-2 function, SMA obtains the optimal values on the F3 function, and the proposed mOPA indicates superior performances on F-4 test functions. Moreover, for the hybrid F-5, F-6, and F-7 test functions, the proposed mOPA algorithm is performing better than the remaining algorithms. For the composite functions F-8, F-9, and F-10, the mOPA outperforms other algorithms and gives the optimal values for F-8 and F-9. In contrast, the original OPA achieves the optimal values for the F-10 test function. Generally, the results demonstrated that mOPA outperformed other algorithms in solving eight of the CEC'2020 benchmark functions in terms of mean, standard deviation, and best and worst values. Additionally, mOPA acquired the first rank in the Friedman mean rank-sum test.

5.2.3 Boxplots behavior analysis

Boxplots are regarded as effective analysis tools because they interpret the data distributions to quartiles to show the realistic distribution of the data in a graphical

Table 4 Parametrization of mOPA and the compared algorithms

Algorithms	Parameters setting
Common settings	Population size: $N = 30$
	Maximum iterations: $\max_{Itr} = 1000$
	Dimensions dim $= 10$
	Number of independent runs: 30
WOA	α decreases linearly from 2 to 0 (Default)
	$a2$ linearly decreases from -1 to -2 (default)
SCA	$A = 2$ (default)
TSA	$P_{min} = 1, P\max = 4$ (default)
SMA	$z = 0.03$ (default)
HHO	$E0 = 1.67, E1 = 1, beta = 1.5$
RUN	$a = 20$ and $b = 12$ (default)
OPA	$p_1 = 0.1, q = 0.9, and\ F = 2$ (default)
mOPA	$p_1 = 0.1, q = 0.9, and\ F = 2$ (default)

representation. We displayed the data distribution with boxplots to further analyze the results of Table 6. The algorithm's minimum and maximum data points constitute the lowest and highest whisker's edges. The ends of the rectangles separate the low and high quartiles. A narrow boxplot indicates a high level of data agreement. Figure 9 presents the boxplots of the data for CEC 2020 test functions from F-1 to F-10 for Dim = 10. The boxplots of mOPA are pretty narrow for most functions, with the lowest values among all comparison algorithms. It is noticed that the distribution of boxplots achieved by the mOPA algorithm is narrower for most test functions and achieves the minimum values compared to the other algorithms. The boxplot graphics shows that the mOPA algorithm consistently finds the best locations for solving the test problems.

5.2.4 Convergence behavior analysis

This subsection analyzes the convergence of the algorithms; Fig. 10 shows the convergence performances of the WOA, SCA, TSA, SMA, HHO, RUN, and OPA against the proposed mOPA for the CEC 2020 test problems for dimension 10. In Fig. 10a, the convergence curves of the F-1 function with a unimodal space are presented. The mOPA method shows an early exploration rather than the original OPA algorithm. Over the test functions of F-2–F-4 with multimodal functions, as shown in Fig. 10b–d, the mOPA exhibits a significant performance through the remaining algorithms for F-3 and F-4, while the RUN algorithm shows a significant performance for the F-2 test function. So, the mOPA has better results in handling the hybrid functions, as shown in Fig. 10e–g, for F-5, F-6, and F-7. The composition functions (F-8, F-9, and F-10), as presented in Fig. 10h–j, exhibited that the proposed mOPA obtains comparative performance in solving problems with complex spaces.

5.2.5 Qualitative metric analysis

Figure 11 presents the qualitative analysis of mOPA on CEC'20. The agent's behaviors are depicted in Fig. 11, which includes a two-dimensional (2D) representation of the functions, search history, average fitness history, optimization history, and diversity. The dimension of these functions is 10. The parameters for the mOPA are the same as in the previous experiment.

***From the qualitative analysis, the following points are remarkable:***

- *According to the domain's topology* The first column in Fig. 11 displays the function in 2D space. The functions have a specific structure that equips sense to decide

Table 5 CEC'20 functions

Test function	Function type	Fi*
Unimodal function		
F-1	Shifted and rotated bent cigar function	100
Multimodal shifted and rotated functions		
F-2	Shifted and rotated Schwefel's function	1100
F-3	Shifted and rotated Lunacek bi-Rastrigin function	700
F-4	Expanded rosenbrock's plus Griewangk's function	1900
Hybrid functions		
F-5	Hybrid–Fun. No.5 ($N = 3$)	1700
F-6	Hybrid–Fun. No.6 ($N = 4$)	1600
F-7	Hybrid–Fun. No.7 ($N = 5$)	2100
Composition functions		
F-8	Composition–Fun. No.8 ($N = 3$)	2200
F-9	Composition–Fun. No.9 ($N = 4$)	2400
F-10	Composition–Fun. No.10 ($N = 5$)	2500
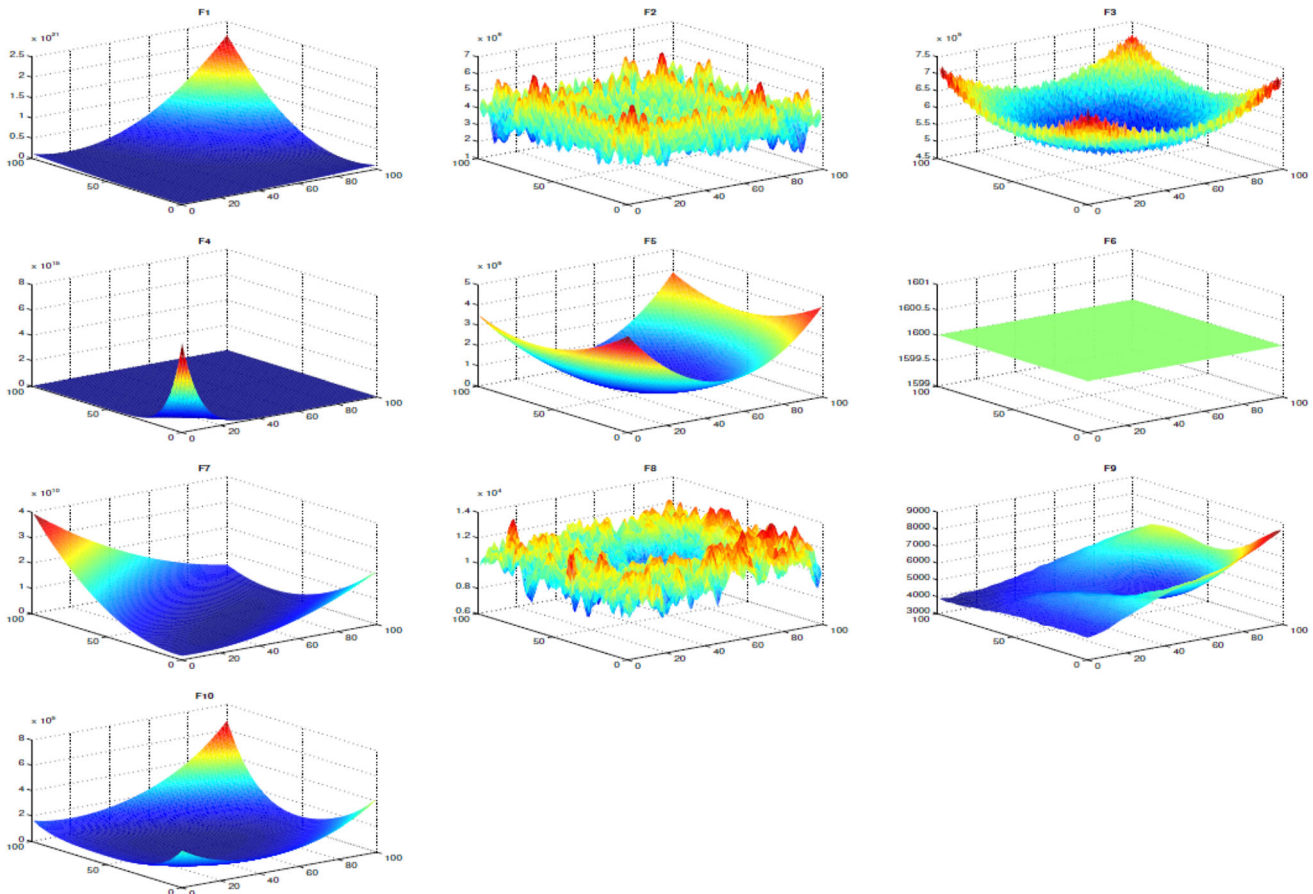
Fig. 8 The two dimensional of the CEC-2020 benchmarks

which functions the algorithm produces the better performance.

- *According to the search history* The search history of agents for all iterations is displayed in the second column of Fig. 11. The search history indicates that

mOPA can determine the regions with the lowest fitness values for some functions.

- *Regarding the average fitness history* The third column of Fig. 11 equips the average fitness history. This average gives details about the agents' overall behavior

Table 6 The mean, STD, BEST, and WORST of fitness values over 30 experiments acquired by the competitor algorithms on the CEC'2020 functions

Function	Metric	WOA	SCA	TSA	SMA	HHO	RUN	OPA	mOPA
F1	Mean	1.034E+07	9.362E+08	3.310E+09	7.183E+03	5.277E+05	3.399E+03	1.715E+03	**7.762E+02**
	STD	1.124E+07	3.570E+08	3.096E+09	4.575E+03	2.787E+05	2.049E+03	2.433E+03	**1.310E+03**
	Best	8.855E+05	4.128E+08	6.913E+06	3.348E+02	1.704E+05	2.141E+02	1.089E+02	**1.000E+02**
	Worst	4.439E+07	2.410E+09	1.218E+10	1.274E+04	1.645E+06	1.174E+04	1.062E+04	**5.020E+03**
F2	Mean	2.190E+03	2.386E+03	2.281E+03	1.617E+03	2.026E+03	**1.539E+03**	1.757E+03	1.576E+03
	STD	3.469E+02	2.275E+02	3.675E+02	**1.629E+02**	2.901E+02	1.919E+02	2.852E+02	3.514E+02
	Best	1.424E+03	1.963E+03	1.688E+03	1.390E+03	1.567E+03	1.129E+03	1.247E+03	**1.115E+03**
	Worst	2.853E+03	2.757E+03	3.036E+03	**1.956E+03**	2.778E+03	2.072E+03	2.465E+03	2.528E+03
F3	Mean	7.819E+02	7.741E+02	8.014E+02	**7.319E+02**	7.830E+02	7.574E+02	7.594E+02	7.378E+02
	STD	2.306E+01	1.180E+01	2.878E+01	**1.013E+01**	2.101E+01	1.611E+01	2.039E+01	1.752E+01
	Best	7.473E+02	7.537E+02	7.596E+02	7.184E+02	7.448E+02	7.207E+02	7.292E+02	**7.140E+02**
	Worst	8.339E+02	8.072E+02	8.739E+02	7.601E+02	8.228E+02	7.884E+02	8.096E+02	**7.796E+02**
F4	Mean	1.908E+03	1.933E+03	4.411E+04	**1.901E+03**	1.908E+03	1.902E+03	**1.901E+03**	**1.901E+03**
	STD	6.144E+00	3.598E+01	6.526E+04	**4.839E−01**	2.995E+00	8.813E−01	6.486E−01	6.602E−01
	Best	1.902E+03	1.912E+03	1.905E+03	1.901E+03	1.902E+03	**1.900E+03**	1.901E+03	**1.900E+03**
	Worst	1.934E+03	2.099E+03	2.584E+05	1.902E+03	1.916E+03	1.904E+03	1.904E+03	**1.901E+03**
F5	Mean	1.545E+05	4.169E+04	2.206E+05	1.045E+04	4.733E+04	3.997E+03	2.038E+03	**1.982E+03**
	STD	2.609E+05	6.601E+04	2.886E+05	6.644E+03	4.760E+04	1.566E+03	1.850E+02	**1.819E+02**
	Best	3.154E+03	6.444E+03	4.174E+03	2.032E+03	3.693E+03	2.277E+03	1.746E+03	**1.702E+03**
	Worst	1.370E+06	3.703E+05	9.375E+05	1.950E+04	1.853E+05	7.197E+03	2.351E+03	**2.333E+03**
F6	Mean	1.611E+03	1.602E+03	1.634E+03	**1.601E+03**	1.617E+03	**1.601E+03**	1.604E+03	**1.601E+03**
	STD	1.379E+01	3.211E−01	2.703E+01	3.008E−01	9.762E+00	2.694E−01	6.687E+00	**2.233E−01**
	Best	1.601E+03	1.601E+03	1.601E+03	1.600E+03	1.601E+03	1.601E+03	1.601E+03	**1.600E+03**
	Worst	1.662E+03	1.603E+03	1.686E+03	**1.601E+03**	1.635E+03	1.602E+03	1.618E+03	**1.601E+03**
F7	Mean	1.502E+05	1.296E+04	5.014E+04	5.431E+03	1.020E+04	3.996E+03	2.233E+03	**2.190E+03**
	STD	2.238E+05	8.902E+03	7.803E+04	5.609E+03	6.542E+03	2.370E+03	1.323E+02	**8.605E+01**
	Best	3.928E+03	4.232E+03	2.618E+03	2.231E+03	2.749E+03	2.159E+03	2.101E+03	**2.100E+03**
	Worst	1.071E+06	4.194E+04	2.038E+05	2.117E+04	3.037E+04	1.180E+04	2.636E+03	**2.496E+03**
F8	Mean	2.352E+03	2.372E+03	2.580E+03	2.368E+03	2.409E+03	2.307E+03	2.297E+03	**2.300E+03**
	STD	2.004E+02	3.636E+01	1.848E+02	2.339E+02	3.172E+02	4.603E+00	1.639E+01	**1.233E+01**
	Best	2.250E+03	2.291E+03	2.238E+03	**2.225E+03**	2.242E+03	2.301E+03	2.228E+03	2.235E+03
	Worst	3.410E+03	2.457E+03	2.886E+03	3.222E+03	3.706E+03	2.321E+03	2.315E+03	**2.308E+03**
F9	Mean	2.767E+03	2.773E+03	2.832E+03	2.758E+03	2.819E+03	2.746E+03	2.771E+03	**2.719E+03**
	STD	5.511E+01	5.735E+01	7.230E+01	8.147E+00	8.049E+01	**7.398E+00**	5.923E+01	7.483E+01
	Best	2.567E+03	2.544E+03	2.521E+03	2.740E+03	2.501E+03	2.732E+03	2.502E+03	**2.500E+03**
	Worst	2.816E+03	2.809E+03	2.980E+03	2.773E+03	2.954E+03	2.757E+03	2.861E+03	**2.766E+03**
F10	Mean	2.938E+03	2.969E+03	3.000E+03	2.939E+03	2.936E+03	2.918E+03	2.929E+03	**2.931E+03**
	STD	5.787E+01	**2.087E+01**	1.475E+02	2.878E+01	2.717E+01	2.376E+01	3.015E+01	2.163E+01
	Best	2.664E+03	2.928E+03	**2.659E+03**	2.898E+03	2.898E+03	2.898E+03	2.898E+03	2.898E+03
	Worst	3.001E+03	3.027E+03	3.608E+03	3.024E+03	3.027E+03	2.960E+03	3.024E+03	**2.950E+03**
Friedman mean rank		**5.60**	**6.2**	**5.14**	**4.80**	**4.50**	**4.20**	**2.35**	**2.01**
Rank		**7**	**8**	**6**	**5**	**4**	**2**	**3**	**1**

Bold values represent to highlight the best-compared results

and their assistance in the optimization process. The history curves are rising, illustrating that the population is enhanced with each iteration.

- *According to the optimization history* Column no. four of Fig. 11 presents the optimization improvement that conveys 100 fitness achieved from 100 iterations per
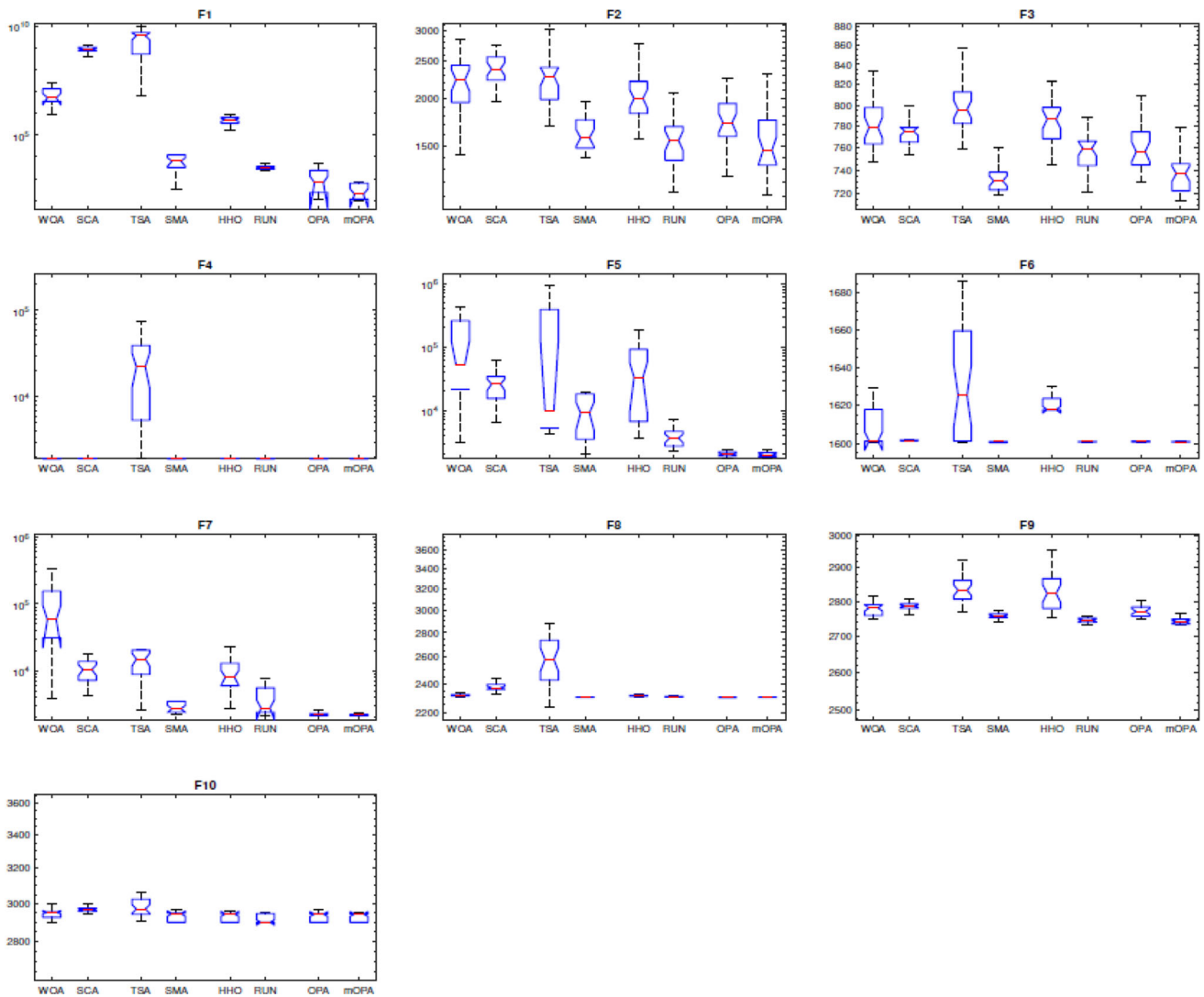
Fig. 9 The boxplot curves of mOPA and the compared algorithms obtained over CEC'20 functions with Dim = 10

experiment to depict the progress of fitness achieved in each iteration. The convergence curves decrease in all test functions, revealing that mOPA has highly with agents during searching for the best solution.

- *According to the diversity metric* The diversity plot is displayed in the last column. The average distance traveled by the agents during the process is shown in this graph.

5.3 Results of the proposed hybrid system

The convergence curves for the optimization process using the mOPA, and the OPA approaches are shown in Fig. 12. These optimization techniques were applied 50 times over 50 iterations to select the proper fitness function rate to regulate the randomness of the suggested techniques, verify their stability, and certify their robustness. All optimization

approach is applied in the same manner for the suggested case study. The developed mOPA consistently identifies the best solution to the optimization issue, as shown by the objective function's final outcomes for the developed mOPA, which fall within a narrow limit.

The suggested enhanced mOPA technique's convergence curve (the best functions profiles with the iterations) is compared to those produced from the original OPA algorithm as well as other conventional optimization methods (MOA, STOA, and SCA) for showing the convergence performance and speed of these techniques. Figure 13 depicts the convergence curves for all these algorithms. As shown in this figure, the proposed mOPA method reaches the final value of the objective function faster than other algorithms. Moreover, the mOPA converges at a lower value of the objective function than the original OPA.
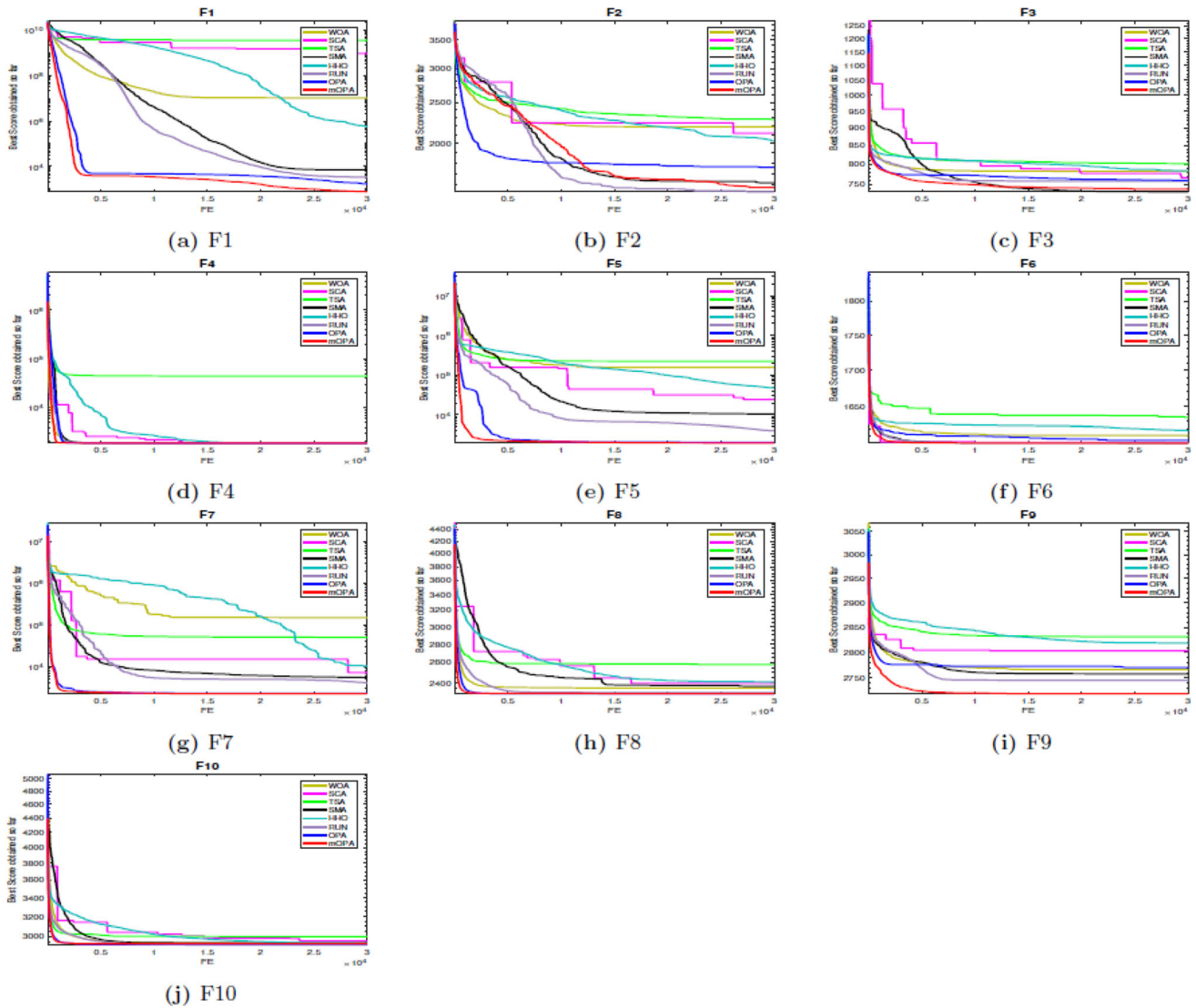
Fig. 10 Convergence curves of mOPA and the compared algorithms on CEC'20 functions with Dim = 10

The sizing and objective function results of the mOPA and OPA algorithms compared to other optimization techniques [12] utilized are indicated in Table 7. This table indicates that the proposed mOPA has the optimal fitness function (0.1219895), followed by OPA (0.12199026), MOA (0.1219998), STOA (0.1221296), and SCA (0.1224865). By comparing the outcomes shown in this table, it can be seen that the suggested mOPA is the best-founded algorithm for optimal sizing of the proposed hybrid system with COE of 0.209626 \$/kWh, followed by OPA, MOA, STOA, and SCA, respectively.

The participation of all components in the annual cost of the suggested hybrid system by utilizing the mOPA and OPA optimization algorithms is shown in Fig. 14. For the two techniques, it is clear that the FC represents the highest annual percentage cost, followed by PV units, ELE units, inverters, BG system, and finally the HT unit.

The proposed hybrid system's power output performance over a 24-hour cycle is shown in Fig. 15. According to the mOPA technique results, the electrolyzer for producing hydrogen is powered by the extra energy from PV and BG units P_{RS}, in case of the generated P_{RS} exceeded the required loads. The P_{dum} will use up this extra power if the HT fills up. While, the FC will use the hydrogen stored in the HT unit to make up for a lack in power generation when the $P'_{RS}s$ output is unable to satisfy the load's power requirements.

For each of the employed optimization algorithms mOPA and OPA, the statistical performance measures are shown in Table 8. For a more precise comparison of the two optimization approaches, parametric and non-parametric statistical measurements were carried out based on the obtained values of the objective function across 50
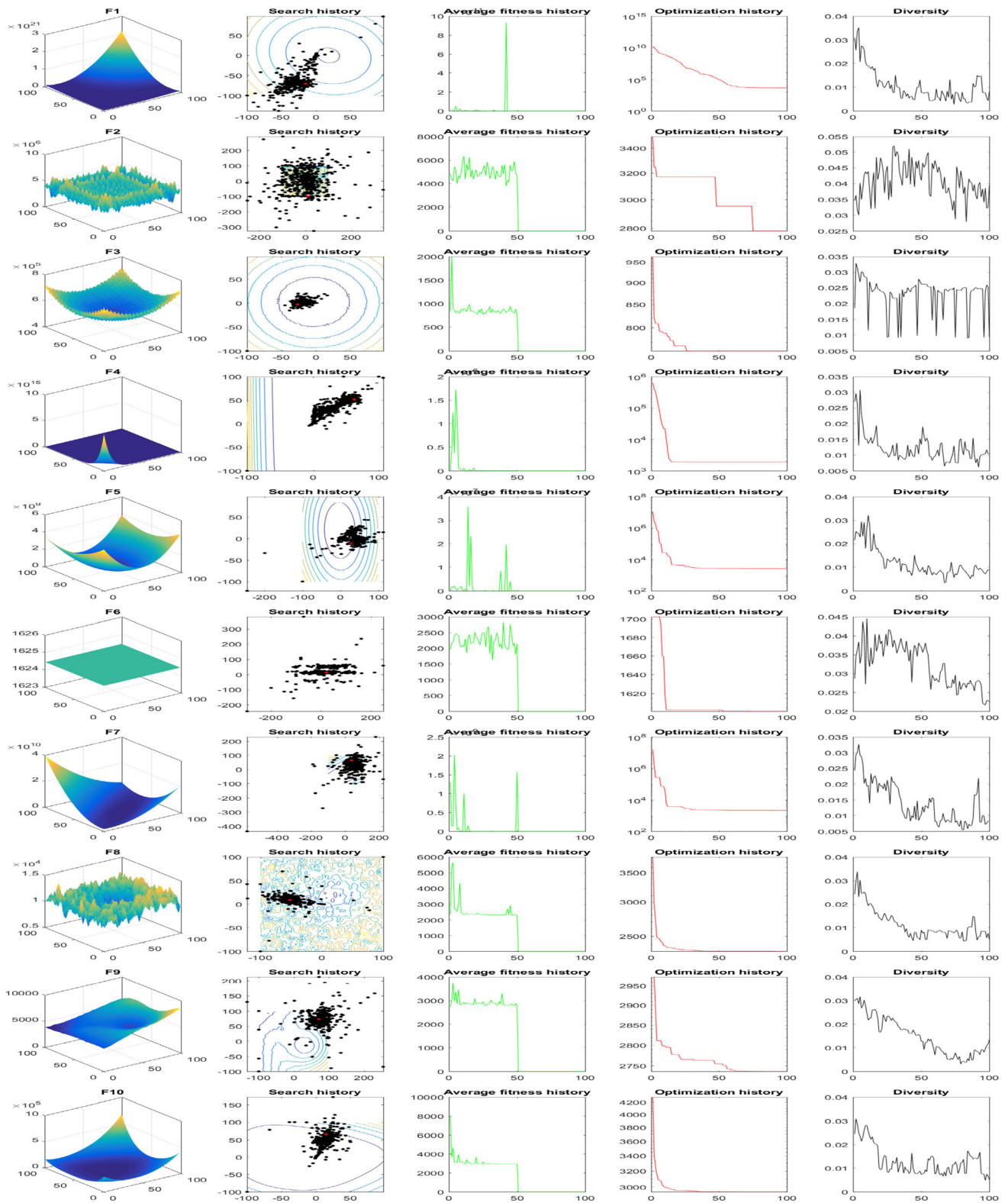
Fig. 11 The qualitative metrics on CEC'20 functions: two-dimensional views of the functions, search history, average fitness history, optimization history, and diversity
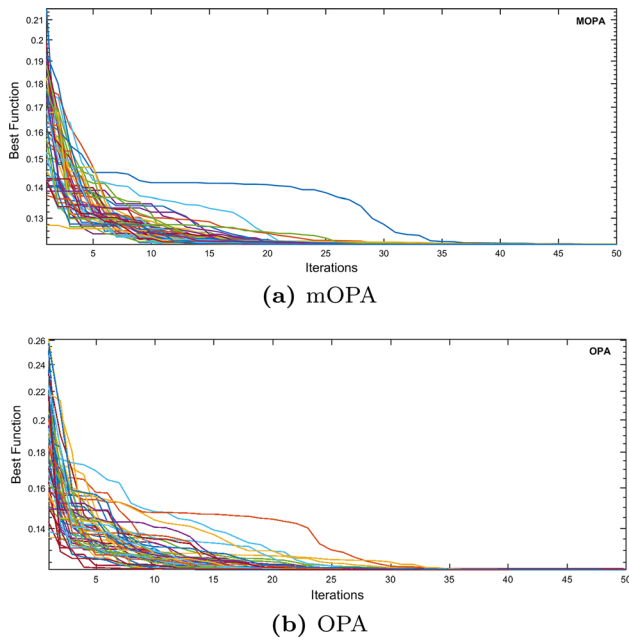
(a) mOPA

(b) OPA

Fig. 12 The convergence curves of the memetic and original Orca Predation Algorithms (mOPA and OPA) for 50 iterations

iterations with 50 distinct runs for the proposed hybrid system. The target function's minimum, maximum, and mean values are all parametric measurements, whereas the efficiency, median, standard deviation, relative error, mean absolute error, and mean absolute error are all non-parametric measurements. Based on the outcomes, the suggested mOPA outperformed the original OPA optimization technique in terms of best values.

Figure 16 displays the graphical representation of the end values of the objective function over 50 individual executions for the proposed hybrid system using the recommended mOPA and the original OPA techniques. It can be noted that, the suggested mOPA's fitness values fell within a specific range, demonstrating the suggested technique's superior stability to the competing techniques. Consequently, using the mOPA optimizer compared to the original OPA optimizer results in better parametric and nonparametric metric values.
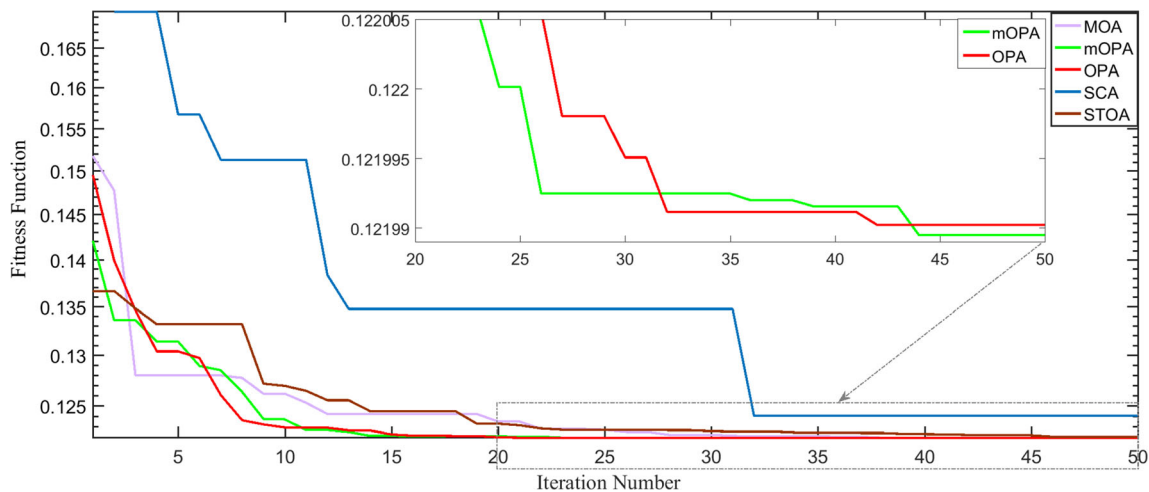
Fig. 13 The optimal convergence curves of the all optimization techniques for 50 iteration

Table 7 The optimization characteristics parameters using mOPA, OPA, MOA, STOA, and SCA methods

| Criteria	mOPA	OPA	MOA [12]	STOA [12]	SCA [12]
Best function	0.1219895	0.12199026	0.1219998	0.1221296	0.1224865
Iteration number	49	11	44	41	27
PV (units)	48	48	47	42	40
BG (units)	2	2	2	2	3
m_{HT} (kg)	62	61.73	62.48	61.28	66.15
$P_{ELE/HT}$ (kW)	320.16	320.32	319.87	326.35	323.419
P_{FC} (kW)	124	124.125	124.71	130.09	134.927
COE ($/kWh)	0.209626	0.2103765	0.2106533	0.210961	0.2123484
NPC ($)	6,140,053	6,162,026	6,170,134	6,179,148	6,219,783
LPSP	0.059926	0.060256	0.05993	0.059411	0.059187
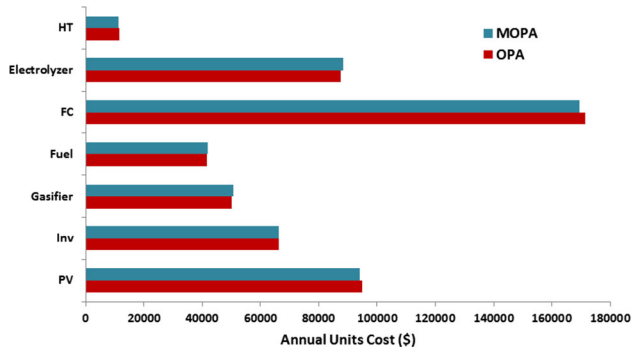
Fig. 14 The annual cost of the proposed system's parts using mOPA and OPA techniques

Table 8 The statistical performance of the mOPA and OPA methods

	mOPA	OPA
Max.	0.1220952	0.1223985
Min.	0.1219895	0.1219902
Mean	0.1220101	0.1220281
Median	0.1219994	0.1220065
SD	0.0026219	0.0065250
RE	0.0084216	0.0156583
MAE	0.0000206	0.0000382
RMSE	0.0000331	0.0000751
Efficiency	99.98316	99.96872

6 Conclusion and future work

This paper proposes a new improved optimization algorithm based on modifying the original Orca Predation Algorithm (OPA) which is a hybrid between two methods, namely, Lévy flight (LF) and opposition-based learning (OBL). This modified algorithm is called mOPA. The mOPA's performance is evaluated on the CEC'2020 test suit. It was applied to an isolated hybrid power system to obtain its optimal sizing. The proposed system consists of photovoltaic panels (PV), biomass gasifier (BG), electrolyzer units (ELE), hydrogen tank units (HT), and fuel cells (FC) to meet the load demand in the Abu-Monqar region, in Egypt. The main objectives of the mOPA method are to minimize energy cost (COE), the loss of power supply probability (LPSP), and excess energy under the constraints of the suggested hybrid system. In order to demonstrate the effectiveness of the mOPA methodology, the optimization results from other algorithms, including the original OPA, Sooty Tern Optimization Algorithm (STOA), and Sine Cosine Algorithm (SCA), were

compared to the mOPA technique's results. Comparisons results illustrate the dominance of the proposed improved mOPA technique against the other metaheuristic methods in obtaining the minimum COE of the proposed hybrid system (the mOPA achieved the best results with the lowest COE by 0.209626\$/kWh, NPC by 6,140,053\$, and LPSP by 0.059926%). Moreover, the recommended mOPA algorithm outperforms the original OPA algorithm in achieving the best minimum values for the objective function as well as the lowest COE value with a quick convergence characteristic and better system performance. Based on the demonstrated results, the recommended mOPA algorithm proved to be more suitable for solving the suggested optimization problem.

Future research may concentrate on the following points:

- Applying the proposed optimization algorithms for solving other complex optimization problems in electrical applications.
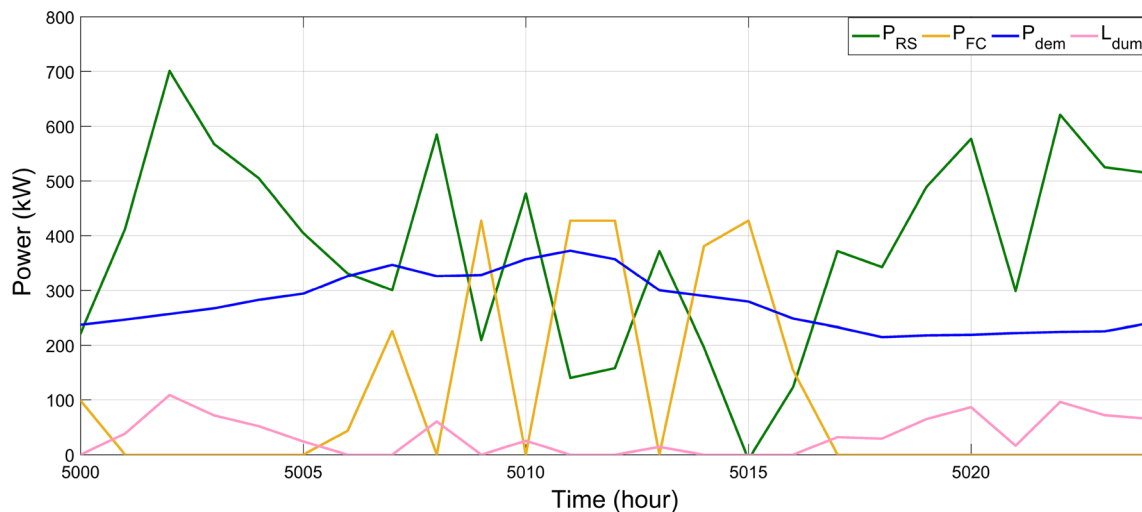

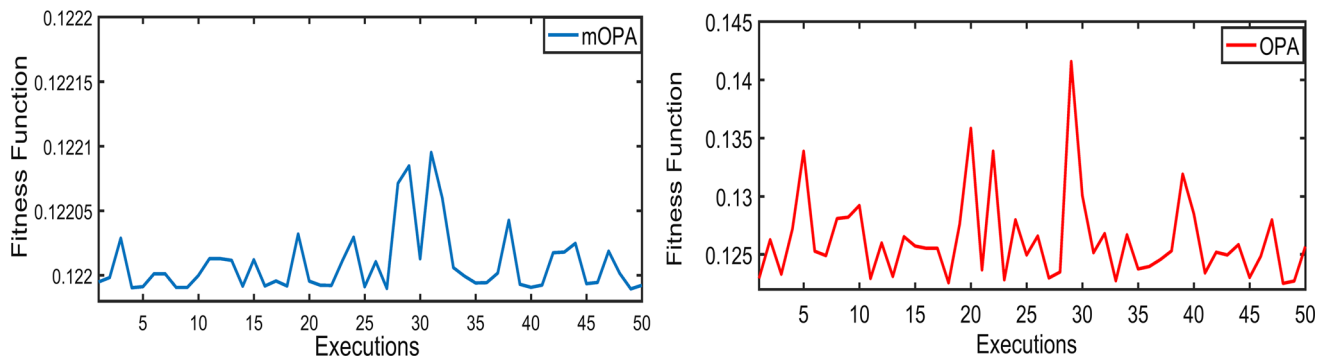**Fig. 15** The operation of the suggested hybrid system during a certain 24 hours using the recommended mOPA

Fig. 16 End values of the objective function of 50 implements

- Using the proposed mOPA algorithm for various real-world applications, such as calculating solar cell parameters, object tracking, hyperparameter optimization, and image segmentation.
- It may be used on the internet of things for task scheduling and preprocessing of data.
- Developing various modeling, operation, and control methods, algorithms, methodologies, and techniques for use in the future development of micro/smart grid technologies.
- Creates a binary version of OPA and applies it to binary problems, such as feature selection problems.
- Determine and investigate the possible configurations of the hybrid renewable systems using different types of storage technologies and components, for effective energy management.

Data availability Data sharing not applicable to this article as no datasets were generated or analyzed during the current study.

Declarations

Conflicts of interest The authors have declared that there are no conflicts of interest.

Ethical standard This article does not contain any studies with human participants or animals performed by any of the authors.

References

1. Ramasamy K, Ravichandran CS (2021) Optimal design of renewable sources of PV/wind/fc generation for power system reliability and cost using MA-RBFN approach. Int J Energy Res 45(7):10946–10962
2. Tezer T, Yaman R, Yaman G (2017) Evaluation of approaches used for optimization of stand-alone hybrid renewable energy systems. Renew Sustain Energy Rev 73:840–853
3. Alturki FA, Al-Shamma'a AA, Farh Hassan MH, AlSharabi K (2021) Optimal sizing of autonomous hybrid energy system using supply-demand-based optimization algorithm. Int J Energy Res 45(1):605–625
4. Fathy Ahmed (2016) A reliable methodology based on mine blast optimization algorithm for optimal sizing of hybrid PV-wind-fc system for remote area in Egypt. Renew Energy 95:367–380
5. Sultan HM, Menesy AS, Kamel S, Korashy A, Almohaimeed SA, Abdel-Akher M (2021) An improved artificial ecosystem optimization algorithm for optimal configuration of a hybrid PV/WT/FC energy system. Alex Eng J 60(1):1001–1025
6. Samy MM, Elkholy Heba I, Barakat S (2021) Multi-objective optimization of hybrid renewable energy system based on biomass and fuel cells. Int J Energy Res 45(6):8214–8230
7. Vendoti S, Muralidhar M, Kiranmayi R (2021) Techno-economic analysis of off-grid solar/wind/biogas/biomass/fuel cell/battery system for electrification in a cluster of villages by homer software. Environ Dev Sustain 23(1):351–372
8. Fathi M, Khezri Rahmat, Yazdani A, Mahmoudi A (2022) Comparative study of metaheuristic algorithms for optimal sizing of standalone microgrids in a remote area community. Neural Comput Appl 34(7):5181–5199
9. Fares D, Fathi M, Mekhilef Saad (2022) Performance evaluation of metaheuristic techniques for optimal sizing of a stand-alone hybrid pv/wind/battery system. Appl Energy 305:117823
10. Abd El-Sattar H, Kamel S, Hassan MH, Jurado F (2022) An effective optimization strategy for design of standalone hybrid renewable energy systems. Energy 260:124901
11. Kharrich M, Abualigah L, Kamel S, AbdEl-Sattar H, Tostado-Véliz Marcos (2022) An improved arithmetic optimization algorithm for design of a microgrid with energy storage system: case study of El Kharga Oasis, Egypt. J Energy Storage 51:104343

12. Abd El-Sattar H, Kamel S, Sultan HM, Zawbaa HM, Jurado F (2022) Optimal design of photovoltaic, biomass, fuel cell, hydrogen tank units and electrolyzer hybrid system for a remote area in Egypt. Energy Rep 8:9506–9527

13. Houssein Essam H, Oliva Diego, Çelik E, Emam MM, Ghoniem RM (2023) Boosted sooty tern optimization algorithm for global optimization and feature selection. Expert Syst Appl 213:119015

14. Hashim FA, Hussain K, Houssein EH, Mabrouk MS, Al-Atabany W (2021) Archimedes optimization algorithm: a new meta-heuristic algorithm for solving optimization problems. Appl Intell 51:1531–1551

15. Eid A, Kamel S, Houssein EH (2022) An enhanced equilibrium optimizer for strategic planning of PV-BES units in radial distribution systems considering time-varying demand. Neural Comput Appl 34(19):17145–17173

16. Houssein EH, Mohamed MH, Mahdy MA, Kamel S (2022) Development and application of equilibrium optimizer for optimal power flow calculation of power system. Appl Intell 53:7232–7253

17. Houssein EH, Abdelkareem DA, Emam MM, Hameed MA, Younan M (2022) An efficient image segmentation method for skin cancer imaging using improved golden jackal optimization algorithm. Comput Biol Med 149:106075

18. Houssein Essam H, Emam Marwa M, Ali Abdelmgeid A (2021) An efficient multilevel thresholding segmentation method for thermography breast cancer imaging based on improved chimp optimization algorithm. Expert Syst Appl 185:115651

19. Houssein Essam H, Emam Marwa M, Ali Abdelmgeid A (2022) An optimized deep learning architecture for breast cancer diagnosis based on improved marine predators algorithm. Neural Comput Appl 34(20):18015–18033

20. Premkumar M, Sowmya R, Ramakrishnan C, Jangir Pradeep, Houssein EH, Deb S, Kumar NM (2023) An efficient and reliable scheduling algorithm for unit commitment scheme in microgrid systems using enhanced mixed integer particle swarm optimizer considering uncertainties. Energy Rep 9:1029–1053

21. Hassan MH, Houssein EH, Mahdy MA, Kamel S (2021) An improved manta ray foraging optimizer for cost-effective emission dispatch problems. Eng Appl Artif Intell 100:104155

22. Mafarja M, Thaher T, Too J, Chantar H, Turabieh H, Houssein EH, Emam MM (2022) An efficient high-dimensional feature selection approach driven by enhanced multi-strategy grey wolf optimizer for biological data classification. Neural Comput Appl 35:1–27

23. Houssein Essam H, Hosney Mosa E, Mohamed Waleed M, Ali Abdelmgeid A, Younis Eman MG (2022) Fuzzy-based hunger games search algorithm for global optimization and feature selection using medical data. Neural Comput Appl 35:1–25

24. Houssein Essam H, Emam Marwa M, Ali Abdelmgeid A (2021) Improved manta ray foraging optimization for multi-level thresholding using Covid-19 CT images. Neural Comput Appl 33(24):16899–16919

25. Emam Marwa M, Houssein Essam H, Ghoniem Rania M (2023) A modified reptile search algorithm for global optimization and image segmentation: case study brain MRI images. Comput Biol Med 152:106404

26. Kennedy J, Eberhart R(1995) Particle swarm optimization. In *Proceedings of ICNN'95-international conference on neural networks*, volume 4, pp 1942–1948. IEEE

27. Holland John H (1992) Genetic algorithms. Sci Am 267(1):66–73

28. Storn R, Price Kenneth (1997) Differential evolution-a simple and efficient heuristic for global optimization over continuous spaces. J Global Optim 11(4):341–359

29. Rashedi E, Nezamabadi-Pour H, Saryazdi S (2009) GSA: a gravitational search algorithm. Inf Sci 179(13):2232–2248

30. Mirjalili S, Mirjalili SM, Hatamlou A (2016) Multi-verse optimizer: a nature-inspired algorithm for global optimization. Neural Comput Appl 27(2):495–513

31. Ahmadianfar I, Bozorg-Haddad O, Chu X (2020) Gradient-based optimizer: a new metaheuristic optimization algorithm. Inf Sci 540:131–159

32. Blum C, Puchinger J, Raidl GR, Roli A (2011) Hybrid meta-heuristics in combinatorial optimization: a survey. Appl Soft Comput 11(6):4135–4151

33. Naik MK, Panda R (2016) A novel adaptive cuckoo search algorithm for intrinsic discriminant analysis based face recognition. Appl Soft Comput 38:661–675

34. Farnad B, Jafarian A, Baleanu Dumitru (2018) A new hybrid algorithm for continuous optimization problem. Appl Math Model 55:652–673

35. Khalilpourazari S, Khalilpourazary S (2019) An efficient hybrid algorithm based on water cycle and moth-flame optimization algorithms for solving numerical and constrained engineering optimization problems. Soft Comput 23(5):1699–1722

36. Ewees AA, Abd Elaziz M, Houssein EH (2018) Improved grasshopper optimization algorithm using opposition-based learning. Expert Syst Appl 112:156–172

37. Aarts E, Aarts EHL, Lenstra JK (2003) Local search in combinatorial optimization. Princeton University Press

38. Rojas-Morales N, Rojas MCR, Ureta EM (2017) A survey and classification of opposition-based metaheuristics. Comput Ind Eng 110:424–435

39. Jiang Y, Wu Q, Zhu S, Zhang L (2022) Orca predation algorithm: a novel bio-inspired algorithm for global optimization problems. Expert Syst Appl 188:116026

40. Tizhoosh Hamid R (2005) Opposition-based learning: a new scheme for machine intelligence. In *Computational intelligence for modelling, control and automation, 2005 and international conference on intelligent agents, web technologies and internet commerce, international conference on*, volume 1, pp 695–701. IEEE

41. Tubishat M, Idris N, Shuib L, Abushariah MA, Mirjalili S (2020) Improved SALP swarm algorithm based on opposition based learning and novel local search algorithm for feature selection. Expert Syst Appl 145:113122

42. Abd Elaziz M, Oliva D, Xiong S (2017) An improved opposition-based sine cosine algorithm for global optimization. Expert Syst Appl 90:484–500

43. Houssein EH, Saad MR, Hashim FA, Shaban H, Hassaballah M (2020) Lévy flight distribution: a new metaheuristic algorithm for solving engineering optimization problems. Eng Appl Artif Intell 94:103731

44. Faramarzi A, Heidarinejad M, Mirjalili S, Gandomi AH (2020) Marine predators algorithm: a nature-inspired metaheuristic. Expert Syst Appl 152:113377

45. Yang X-S (2010) Engineering optimization: an introduction with metaheuristic applications. John Wiley

46. Mantegna RN (1994) Fast, accurate algorithm for numerical simulation of levy stable stochastic processes. Phys Rev E 49(5):4677

47. Maleki A, Alhuyi NM, Pourfayaz F (2020) Harmony search optimization for optimum sizing of hybrid solar schemes based on battery storage unit. Energy Rep 6:102–111

48. Bukar AL, Tan CW, Lau KY (2019) Optimal sizing of an autonomous photovoltaic/wind/battery/diesel generator microgrid using grasshopper optimization algorithm. Solar Energy 188:685–696

49. Sultan Hamdy M, Kuznetsov Oleg N, Menesy Ahmed S, Kamel Salah (2020) Optimal configuration of a grid-connected hybrid pv/wind/hydro-pumped storage power system based on a novel optimization algorithm. In *2020 International Youth Conference*

on *Radio Electronics, Electrical and Power Engineering (REEPE)*, pages 1–7. IEEE, 2020

50. El-Sattar Abd H, Kamel S, Tawfik M A, Vera D, Jurado F (2019) et al. Modeling and simulation of corn stover gasifier and microturbine for power generation. *Waste Biomass Valoriz*, 10: 3101–3114

51. Eteiba MB, Barakat S, Samy MM, Wahba WI (2018) Optimization of an off-grid PV/biomass hybrid system with different battery technologies. Sustain Cities Soc 40:713–727

52. Cano A, Arévalo P, Jurado F (2020) Energy analysis and techno-economic assessment of a hybrid PV/HKT/bat system using biomass gasifier: Cuenca-Ecuador case study. Energy 202:117727

53. Kashefi Kaviani A, Riahy GH, Kouhsari SHM (2009) Optimal design of a reliable hydrogen-based stand-alone wind/PV generating system, considering component outages. Renew Energy 34(11):2380–2390

54. Nelson DB, Nehrir MH, Wang C (2006) Unit sizing and cost analysis of stand-alone hybrid wind/PV/fuel cell power generation systems. Renew Energy 31(10):1641–1656

55. Baghaee HR, Mirsalim M, Gharehpetian GB, Talebi HA (2016) Reliability/cost-based multi-objective pareto optimal design of stand-alone wind/PV/FC generation microgrid system. Energy 115:1022–1041

56. Abd El-Sattar H, Kamel S, Hassan MH, Jurado F (2022) Optimal sizing of an off-grid hybrid photovoltaic/biomass gasifier/battery system using a quantum model of Runge Kutta algorithm. Energy Convers Manag 258:115539

57. Houssein Essam H, Çelik E, Mahdy Mohamed A, Ghoniem Rania M (2022) Self-adaptive equilibrium optimizer for solving global, combinatorial, engineering, and multi-objective problems. Expert Syst Appl 195:116552

58. Mirjalili S, Lewis A (2016) The whale optimization algorithm. Adv Eng Softw 95:51–67

59. Mirjalili S (2016) SCA: a sine cosine algorithm for solving optimization problems. Knowl-Based Syst 96:120–133

60. Kaur S, Awasthi LK, Sangal AL, Dhiman G (2020) Tunicate swarm algorithm: a new bio-inspired based metaheuristic paradigm for global optimization. Eng Appl Artif Intell 90:103541

61. Li S, Chen H, Wang M, Heidari AA, Mirjalili S (2020) Slime mould algorithm: a new method for stochastic optimization. Future Gener Comput Syst 111:300–323

62. Heidari AA, Mirjalili S, Faris H, Aljarah I, Mafarja M, Chen H (2019) Harris Hawks optimization: algorithm and applications. Future Gener Comp Syst 97:849–872

63. Ahmadianfar I, Heidari AA, Gandomi AH, Chu X, Chen H (2021) Run beyond the metaphor: an efficient optimization algorithm based on Runge Kutta method. Expert Syst Appl 181:115079

64. Arcuri A, Fraser G (2013) Parameter tuning or default values? an empirical investigation in search-based software engineering. Empir Softw Eng 18(3):594–623

65. Zitouni F, Harous S, Maamri R (2021) The solar system algorithm: a novel metaheuristic method for global optimization. IEEE Access 9:4542–4565